

1 **Microstructure and carbon storage capacity of hydrated magnesium carbonates**
2 **synthesized from different sources and conditions**

3
4 Haoliang Dong^a, Cise Unluer^a, En-Hua Yang^{a,*}, Fei Jin^b, Abir Al-Tabbaa^b

5
6 ^a School of Civil and Environmental Engineering, Nanyang Technological University, 50
7 Nanyang Avenue, Singapore 639798, Singapore

8 ^b Department of Engineering, University of Cambridge, Trumpington Street, Cambridge CB2
9 1PZ, UK

10
11 **Abstract**

12 Recently, the mineral carbonation via the reaction of CO₂ with saline aquifers received much
13 attention as one of the most promising ways for geologic CO₂ storage. This paper reports
14 microstructure and carbon storage capacity of hydrated magnesium carbonates (HMCs)
15 synthesized from different sources, *i.e.*, reject brine and commercial Mg(OH)₂ slurry, and under
16 different conditions, *i.e.*, pH (8-14) and Mg(OH)₂:CO₂ molar ratio (1:1-1:7). Results show that
17 dypingite (Mg₅(CO₃)₄(OH)₂·5H₂O) is the main phase forming at lower Mg(OH)₂:CO₂ ratios.
18 An increase in the Mg(OH)₂:CO₂ ratio and/or pH leads to the precipitation of nesquehonite
19 (MgCO₃·3H₂O). A unique “house of cards” texture, involving formation of the rosette-like
20 dypingite flakes on the surface of nesquehonite needles, is discovered under elevated pH and
21 Mg(OH)₂:CO₂ ratios. HMCs synthesized from reject brine exhibit a much higher carbon
22 storage capacity of 82.6% than that produced from the commercial Mg(OH)₂ slurry (43.7%).

* Corresponding author. Address: N1-01b-56, 50 Nanyang Avenue, Singapore 639798. Tel.: +65 6790 5291;
fax: +65 6791 0676. *E-mail*: ehyang@ntu.edu.sg

23 Findings from this study advance understanding of mineral recovery from reject brine and the
24 capture and long-term storage of CO₂ in the form of HMCs.

25

26 **Keywords:** *Reject brine; Mg(OH)₂; pH; hydrated magnesium carbonates (HMCs); carbon*
27 *capture and storage*

28

29 **1. Introduction**

30 Fossil fuels have been the world's primary energy source, providing over 85% of the energy
31 demands worldwide [1-6]. However, nearly 83% of the anthropogenic greenhouse gas (GHG)
32 emissions are coming from combustion and non-fuel uses of fossil fuels [7]. CO₂, which is the
33 main GHG, has caused most of the global warming since it has the highest positive radiative
34 forcing and far more abundant in the atmosphere than other heat-trapping gases [8, 9]. The
35 concentration of CO₂ in the atmosphere has increased ~30% from 325 parts per million (ppm)
36 at the beginning of the industrial era in 1970 to 409.7 ppm in May 2017 measured in Mauna
37 Loa Observatory. Consequently, much attention has been drawn to the carbon management
38 [10-12]. Carbon capture and storage (CCS) provides a feasible way to reduce the build-up of
39 CO₂ in the atmosphere [13, 14]. CCS concept covers broad fields such as ocean, terrestrial,
40 geological, biological and chemical approaches to store CO₂ gas in the long term [15-18],
41 among which mineral carbonation via the reaction of CO₂ with saline aquifers is one of the
42 most promising geologic CO₂ storage options [19-23]. Magnesium-based minerals have
43 attracted great attentions worldwide as they show the potential to sequester anthropogenic
44 CO₂ to counterpart the global warming [24-27]. Furthermore, reactive magnesia (MgO) cement
45 has been studied as a potential alternative to the Portland cement due to its ability to sequester
46 significant amount of carbon dioxide (CO₂) and potential to be fully recycled [28-32].

47

48 Although the most thermodynamically stable carbonate for magnesium is in the anhydrous
49 form, *i.e.*, magnesite (MgCO_3) [33-35], formation of magnesite at the ambient condition is not
50 common. Instead, formation of hydrated magnesium carbonates (HMCs) prevails as Mg^{2+} ions
51 in the solution are highly hydrated [24]. HMCs are a class of magnesium compounds that form
52 in $\text{MgO-CO}_2\text{-H}_2\text{O}$ systems, where the carbonation of magnesium systems generate a variety of
53 phases, including dypingite ($\text{Mg}_5(\text{CO}_3)_4(\text{OH})_2 \cdot 5\text{H}_2\text{O}$) [36], hydromagnesite
54 ($\text{Mg}_5(\text{CO}_3)_4(\text{OH})_2 \cdot 4\text{H}_2\text{O}$) [37], and nesquehonite ($\text{MgCO}_3 \cdot 3\text{H}_2\text{O}$) [18, 38]. It has been reported
55 that inclusion of HMCs in reactive MgO cement enhances carbonation of the resulting binder
56 [39].

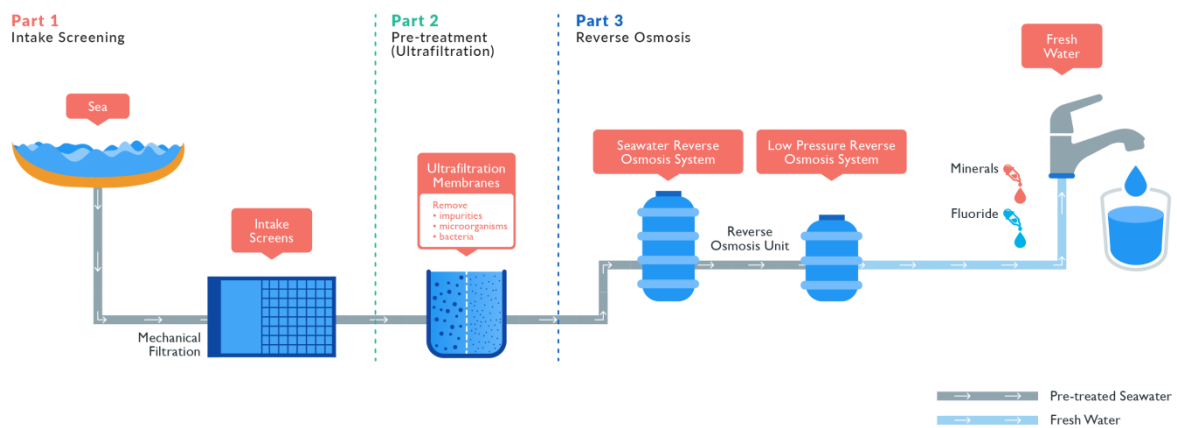
57
58 Theoretically, the formation of different phases of HMCs with different morphologies is
59 influenced by temperature, pH and CO_2 partial pressure [24, 40, 41]. Recent experimental
60 studies show that the precipitation of nesquehonite with needle-like morphology in an aqueous
61 solution occurs commonly under ambient conditions [15, 18, 38]. As the reaction temperatures
62 (333-368 K) and pH values increased, needle-like nesquehonite was replaced by
63 hydromagnesite with sheet-like morphology since nesquehonite is widely known to transform
64 to hydromagnesite at temperature above 50°C [40]. Hydromagnesite was reported to form at
65 120°C and P_{CO_2} of 3 bar, which gradually transformed to magnesite within 5-15 hours.
66 However, a further increase of P_{CO_2} to 100 bar at 120°C resulted in the direct precipitation of
67 magnesite [24]. The thermal behavior of the synthesized HMCs (*e.g.*, nesquehonite) has been
68 tested through real time in-situ X-ray diffraction (XRD), which indicated that nesquehonite and
69 dypingite remained thermal and structural stable up to 373 K and 435 K, respectively [36, 42].
70 Under the continued thermal treatment, nesquehonite transited into magnesite which was even
71 thermally stable up to 600 K, while dypingite transited into hydromagnesite at around 570 K,
72 assuring the long-term storage of CO_2 . However, the influences of $\text{Mg}(\text{OH})_2/\text{CO}_2$ molar ratios

73 and pH on the phases, morphology, and CCS efficiency of HMCs have yet been studied
74 systematically.

75

76 Desalination is a process that removes minerals from saline water. In coastal regions such as
77 Singapore where sources of fresh water are limited, desalination provides a feasible option to
78 produce fresh water. However, a high salty waste stream (*i.e.*, reject brine) would be generated
79 as much as the produced desalinated water at the end of the process [43]. Reject brine is a much
80 more complex media because chemicals are often added into the intake seawater (*e.g.*, to
81 precipitate the colloidal particles before running through the ultra-filtration) in the desalination
82 process (Fig. 1). Although many studies have investigated mineral trapping of CO₂ into saline
83 aquifers (*e.g.*, seawater, natural brine, or synthesized MgCl₂ solution) [18, 36, 42, 44-46], very
84 few has reported the use of reject brine as the CO₂ reservoir [47] and no study has proposed to
85 use reject brine as the Mg(OH)₂ source to synthesize HMCs.

86



87

88 Figure 1 Schematic illustration of the typical process in a reverse osmosis desalination plant

89

[48]

90

91 In this paper, influence of key parameters including $\text{Mg}(\text{OH})_2:\text{CO}_2$ molar ratio, pH, and
92 $\text{Mg}(\text{OH})_2$ source on HMCs synthesis were investigated. The resulting HMCs were
93 characterized by means of XRD, scanning electron microscopy (SEM), and
94 thermogravimetric/differential thermal analysis (TG/DTA) to reveal phases, morphology, and
95 CCS efficiency of HMCs synthesized under different conditions. In the following sections,
96 materials and methodologies are presented first, followed by results presentation and
97 discussion.

98

99 **2. Materials and Methodology**

100 **2.1. Materials**

101 Reject brine sample was collected from a local desalination plant which generates 318,500 m³
102 desalinated water per day. The sample was filtrated through a 45 μm membrane filter to remove
103 suspended solids before further analysis. An inductively coupled plasma-optical emission
104 spectroscopy (ICP-OES) was used to analyze the chemical composition of reject brine in the
105 current study (Table 1). Analytical grade $\text{Mg}(\text{OH})_2$ (92% pure) and analytical grade sodium
106 hydroxide (NaOH) with a purity of 97% were both purchased from VWR Pte Ltd in Singapore.
107 Compressed CO_2 was purchased from Leeden National Oxygen Ltd in Singapore.

108

109 Table 1 Chemical composition of reject brine

Element	Cl	Na	SO_4	Mg	K	Ca	Sr	B	Si	Li	P	Al
Concentration (ppm)	65593	13580	4323	1718	846	471	14.6	3.8	3.7	0.3	0.2	0.1

110

111 **2.2. Methodology**

112 In the first approach, 0.82 g commercially available analytical grade $\text{Mg}(\text{OH})_2$ was dissolved
113 into 200 ml ultra-pure water to prepare the $\text{Mg}(\text{OH})_2$ slurry. To study the influences of

114 $\text{Mg}(\text{OH})_2/\text{CO}_2$ molar ratios and pH on the microstructures of HMCs , three sets of experiments
115 were designed at controlled conditions, *i.e.*, $\text{Mg}(\text{OH})_2:\text{CO}_2$ molar ratio (1:1-1:7) and pH (8-14).
116 CO_2 was sparged into the slurry at a rate of 100 ml/min at room temperature under pre-
117 determined conditions as follows,

118 a) pH = 8, $\text{Mg}(\text{OH})_2:\text{CO}_2$ molar ratio = 1:1 to 1:7

119 b) pH = 8 to 11, $\text{Mg}(\text{OH})_2:\text{CO}_2$ molar ratio = 1:1

120 c) pH = 8 to 11, $\text{Mg}(\text{OH})_2:\text{CO}_2$ molar ratio = 1:2

121

122 In the second approach, $\text{Mg}(\text{OH})_2$ was first synthesized from the reject brine via the addition
123 of NaOH at an optimized condition (*i.e.*, NaOH/ Mg^{2+} ratio of 2 at 25°C) determined from our
124 previous work [49-51], which results high yield and high purity $\text{Mg}(\text{OH})_2$. After which, 0.82 g
125 of synthesized $\text{Mg}(\text{OH})_2$ was mixed with 200 ml ultra-pure water. CO_2 was sparged into the
126 slurry at a rate of 100 ml/min at room temperature under controlled condition (*i.e.*, pH = 8,
127 $\text{Mg}(\text{OH})_2:\text{CO}_2$ molar ratio = 1:1).

128

129 A pH/thermometer probe, inserted into reject brine, was used to continuously record the
130 temperature and pH during the experiment. A CO_2 flowmeter was used to monitor and record
131 the volume of CO_2 diffused into the slurry. Once the diffused CO_2 reached the pre-determined
132 value (*i.e.*, calculated based on the designed $\text{Mg}(\text{OH})_2:\text{CO}_2$ molar ratio), the reaction was
133 terminated. 1M NaOH was added into the slurry continuously to maintain the pH to the
134 designed value since sparging CO_2 lowered the pH of slurry. HMCs were separated from the
135 solution by a centrifuge and washed three times using ultra-pure water. The washed samples
136 were fully dried in an oven at low temperature (*i.e.*, 40°C) to avoid any phase changes, before
137 being ground into powder form. The prepared powder was finally passed through a 125 μm
138 sieve for further microstructural analysis.

139

140 ICP-OES (PerkinElmer Optima DV2000) was employed to measure the chemical composition
141 of the reject brine before and after the reactions. The XRD (Bruker D8 Advance) diffractograms
142 of the synthesized HMCs were recorded from 5° to 70° at $0.02^\circ/\text{step}$ with a $\text{CuK}\alpha$ radiation at
143 40 kV and 40 mA. The morphology of the synthesized HMCs was investigated by a field
144 emission SEM (JSM-7600F). TG/DTA (PyrisDiamond 4000) of the synthesized HMCs was
145 operated at a heating rate of $10^\circ\text{C}/\text{min}$ under the air flow condition.

146

147 **3. Results and Discussion**

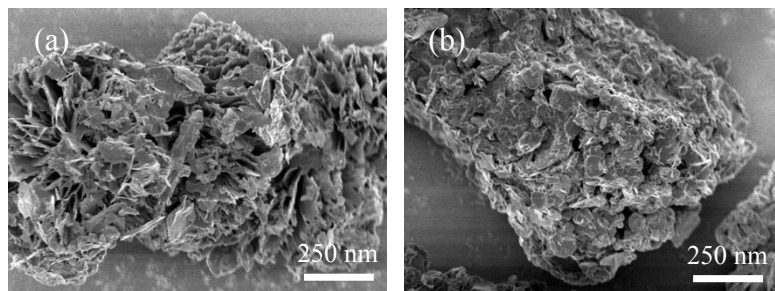
148 **3.1. Characterization of HMCs synthesized from $\text{Mg}(\text{OH})_2$ slurry**

149 **3.1.1. Effect of $\text{Mg}(\text{OH})_2/\text{CO}_2$ molar ratio**

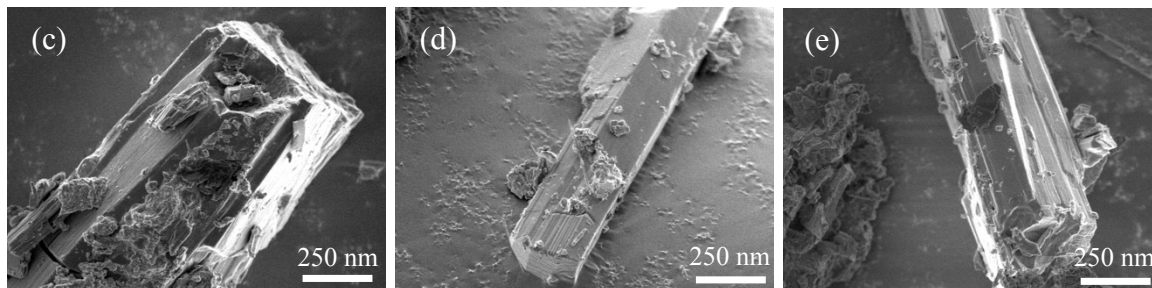
150 Figure 2 shows the FESEM images of all samples obtained under a constant pH of 8 while the
151 $\text{Mg}(\text{OH})_2:\text{CO}_2$ molar ratio was varied between 1:1 and 1:7. The morphologies of the obtained
152 HMCs dramatically changed with the $\text{Mg}(\text{OH})_2:\text{CO}_2$ molar ratio. For instance, the rosette-like
153 morphology observed when the $\text{Mg}(\text{OH})_2:\text{CO}_2$ molar ratio was 1:1 (Fig. 2a), which was
154 eventually replaced by rod-like structures with smooth surfaces when this ratio gradually
155 increased to 1:6 (Figs. 2b-f). The boundaries of these rod-like carbonate phases became clearer
156 with an increase in the $\text{Mg}(\text{OH})_2:\text{CO}_2$ molar ratio. A further increase in the $\text{Mg}(\text{OH})_2:\text{CO}_2$
157 molar ratio to 1:7 revealed the formation of a layer of rosette-like flakes around the original
158 rod-like morphology, producing a “house of cards” texture on the surface [52], as shown in
159 Fig. 2g.

160

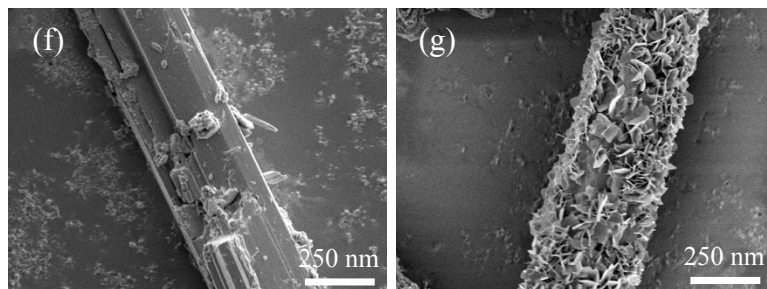
161



162



163



164 Figure 2 FESEM images of HMCs obtained under a pH of 8 at different $\text{Mg}(\text{OH})_2:\text{CO}_2$ molar
 165 ratios of (a) 1:1, (b) 1:2, (c) 1:3, (d) 1:4, (e) 1:5, (f) 1:6 and (g) 1:7

166

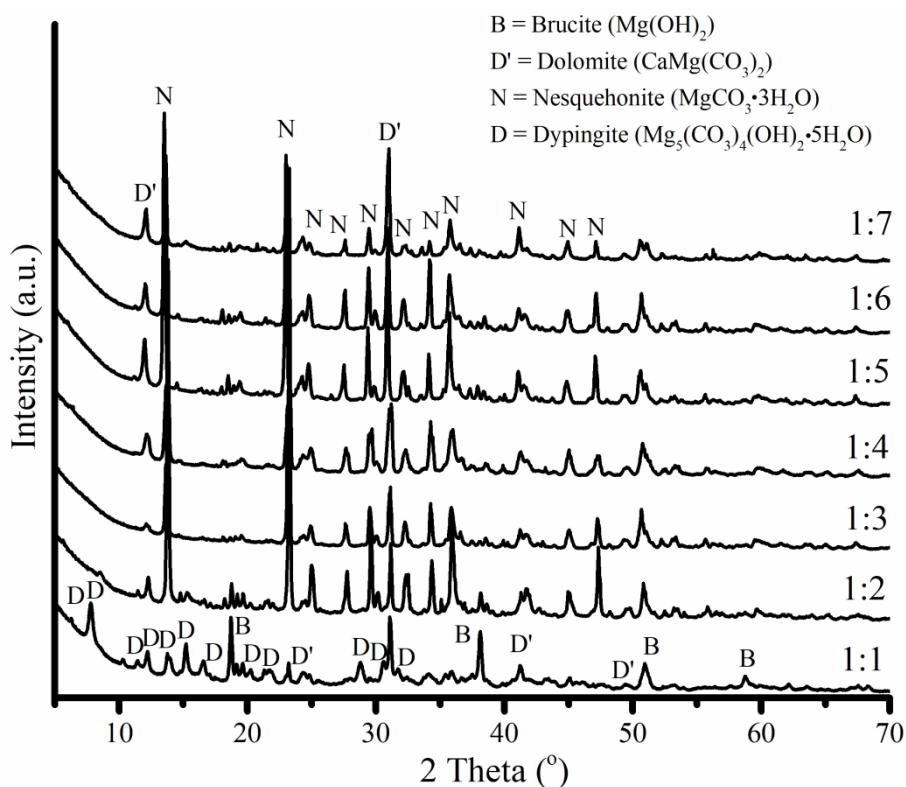
167 Fig. 3 indicates the XRD diffractograms of the same set of samples obtained under a pH of 8
 168 at different $\text{Mg}(\text{OH})_2:\text{CO}_2$ molar ratios. The XRD patterns confirmed that the rosette- and rod-
 169 like particles observed in Fig. 2 could be attributed to dypingite and nesquehonite, respectively.
 170 These morphological observations were in line with the previous literature [18, 36, 41], where
 171 the distinct morphologies of dypingite and nesquehonite were reported. At the $\text{Mg}(\text{OH})_2:\text{CO}_2$
 172 molar ratio of 1:1, the precipitates consisted of dypingite, uncarbonated brucite and dolomite
 173 that was present as an impurity within $\text{Mg}(\text{OH})_2$. An increase in the $\text{Mg}(\text{OH})_2:\text{CO}_2$ molar ratio
 174 to 1:2 revealed a reduction in the amount of uncarbonated brucite, resulting in the domination
 175 of nesquehonite. These results corresponded well with the chemical composition of different

176 carbonate phases. Accordingly, the abundance of nesquehonite could be associated with the
177 availability of higher amounts of CO₂ introduced into the mix under higher Mg(OH)₂:CO₂
178 molar ratios. This is because nesquehonite (MgCO₃·3H₂O) requires a higher Mg:CO₂ molar
179 ratio of 1:1 than dypingite (Mg₅(CO₃)₄(OH)₂·5(H₂O)), which can theoretically form at a
180 corresponding ratio of 1:0.8. Further increase of the Mg(OH)₂:CO₂ molar ratio from 1:2 to 1:7
181 did not lead to significant changes in the XRD patterns, where nesquehonite continued to be
182 the dominate phase which is consistent with the SEM observation (Fig. 2).

183

184 The “house of cards” morphology is related to a dissolution-recrystallization self-assembly
185 growth mechanism when the dissolution rate of nesquehonite was faster than the precipitation
186 rate of hydromagnesite [52]. Thus, the formation of “house of cards” texture on the surface of
187 HMCs synthesized at Mg(OH)₂:CO₂ molar ratio of 1:7 (Fig. 2g) reveals that while
188 nesquehonite is still the dominating phase of the main body (Fig. 3), nesquehonite on the
189 surface was transformed into hydromagnesite phase due to elevated CO₂ concentration.

190



191

192 Figure 3 XRD diffractograms of HMCs obtained under a pH of 8 at different $\text{Mg}(\text{OH})_2:\text{CO}_2$
 193 molar ratios

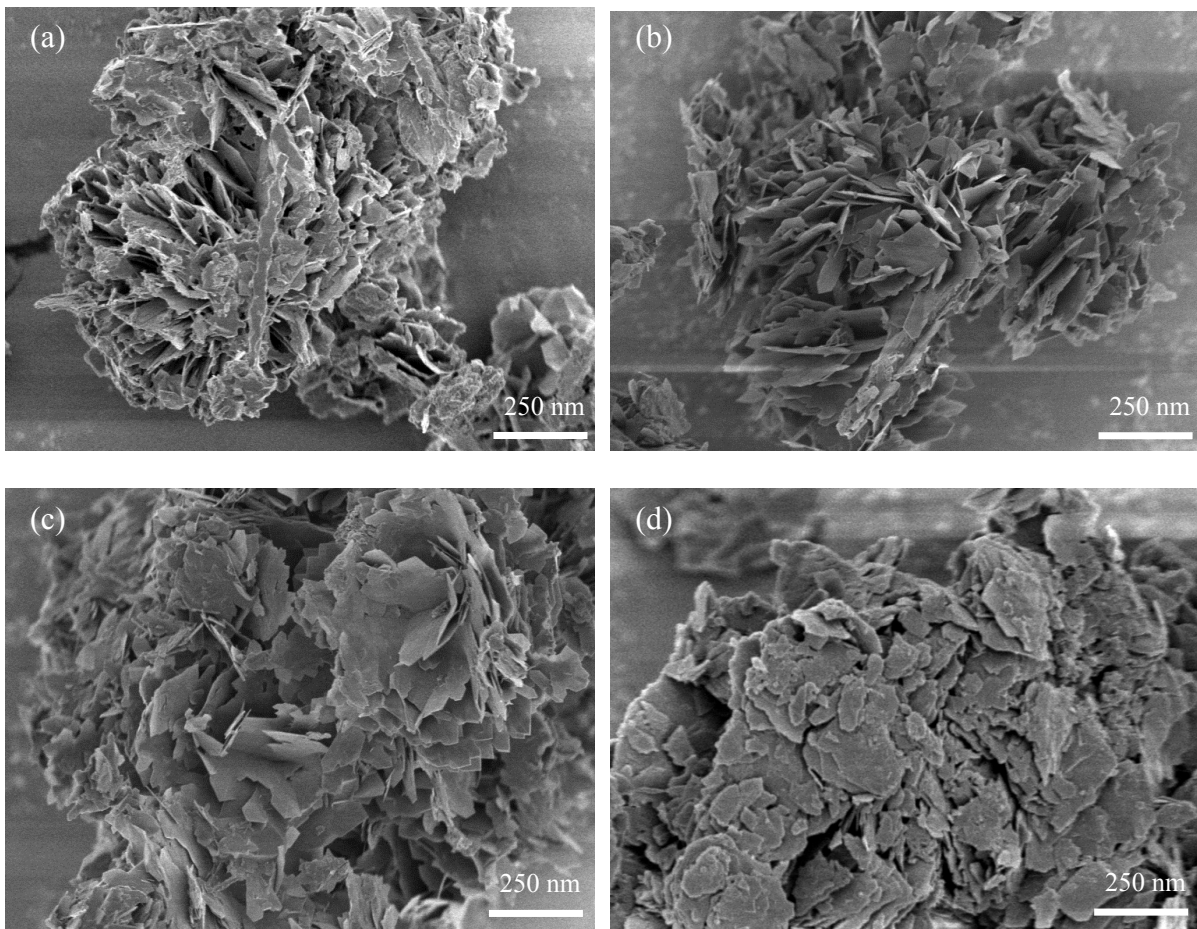
194

195 **3.1.2. Effect of pH at $\text{Mg}(\text{OH})_2$ -to- CO_2 molar ratio of 1**

196 Figure 4 illustrates the FESEM images of the samples obtained under different pH values
 197 ranging between 8 and 11, at a constant $\text{Mg}(\text{OH})_2:\text{CO}_2$ molar ratio of 1:1. At the lower pH
 198 values of < 11 , the obtained carbonates displayed rosette-like morphologies with an average
 199 dimension of $\sim 2 \mu\text{m}$, as shown in Figures 4(a)-(c). These rosette-like formations were
 200 confirmed to be dypingite, as shown by the XRD patterns presented in Figure 5. As the pH
 201 increased from 8 to 10, the intensity of the uncarbonated brucite peak revealed a decrease
 202 relative to the others, possibly indicating a reduction in the amount of brucite and an associated
 203 higher degree of carbonation at elevated pH levels. This increase in the carbonation degree
 204 could be associated with the higher $\text{CO}_3^{2-}:\text{HCO}_3^-$ ratios in the prepared solutions at elevated
 205 pH levels. An increase in the pH led to higher concentrations of OH^- , therefore enabling the

206 conversion of HCO_3^- to CO_3^{2-} , which then reacted with Mg^{2+} , leading to the precipitation of
207 higher amounts of HMCs in the solution. Alternatively, a further increase in the pH from 11 to
208 14 lowered the carbonation degree of brucite, which was observed with its flake-like
209 morphology in Figure 4(d). These results were in line with the findings reported in previous
210 studies, where the optimal pH for the carbonation of brucite was shown to be around 9 [53].

211

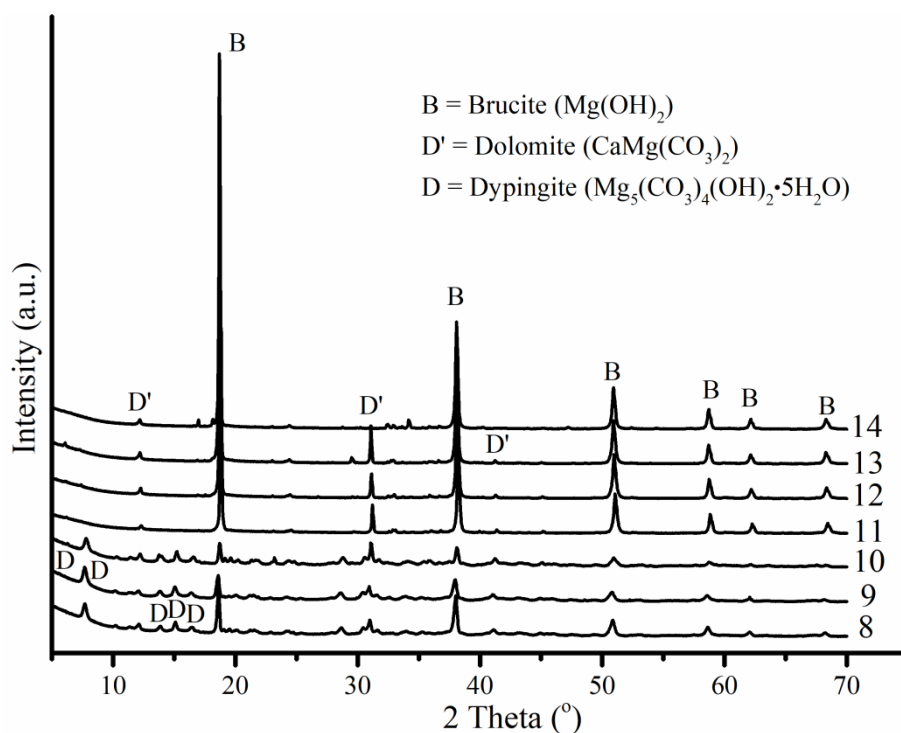


212

213

214 Figure 4 FESEM images of HMCs obtained at the $\text{Mg}(\text{OH})_2:\text{CO}_2$ molar ratio of 1:1 under
215 different pH values of (a) 8, (b) 9, (c) 10 and (d) 11

216



217

218 Figure 5 XRD diffractograms of HMCs obtained at the $\text{Mg}(\text{OH})_2:\text{CO}_2$ molar ratio of 1:1

219 under different pH values

220

221 3.1.3 Effect of pH at $\text{Mg}(\text{OH})_2:\text{CO}_2$ molar ratio of 1:2

222 Figure 6 displays the morphologies of HMCs obtained under different pH values at the

223 $\text{Mg}(\text{OH})_2:\text{CO}_2$ molar ratio of 1:2. Different from HMCs obtained at the $\text{Mg}(\text{OH})_2:\text{CO}_2$ molar

224 ratio of 1:1, where the presence of dypingite with a rosette-like morphology dominated

225 regardless of the pH value; HMCs obtained at the $\text{Mg}(\text{OH})_2:\text{CO}_2$ molar ratio of 1:2 clearly

226 demonstrated a different morphology. Instead of the previously observed rosette-like plates, a

227 rod-like structure presenting the “house of cards” texture was seen in samples obtained under

228 pH values of 8 and 9 (Figs. 6a-b). An increase in the pH from 8 onwards resulted in the

229 distortion of the originally clear borders of the nesquehonite crystals, whose shape transformed

230 from the rod-like structure to a cluster of flakes forming on top. This change was mostly

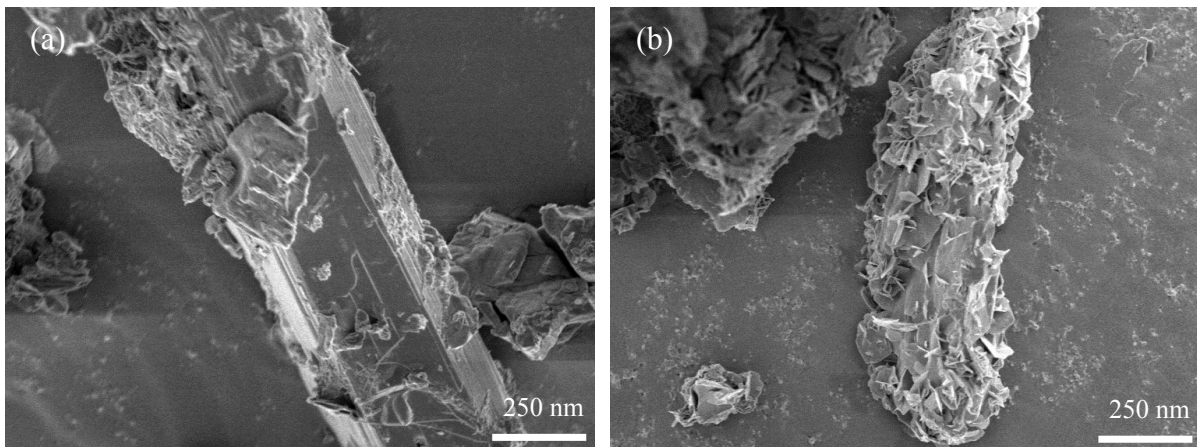
231 obvious at pH values of 10 and 11 (Figures 6(c) and (d)), which revealed the formation of flake-

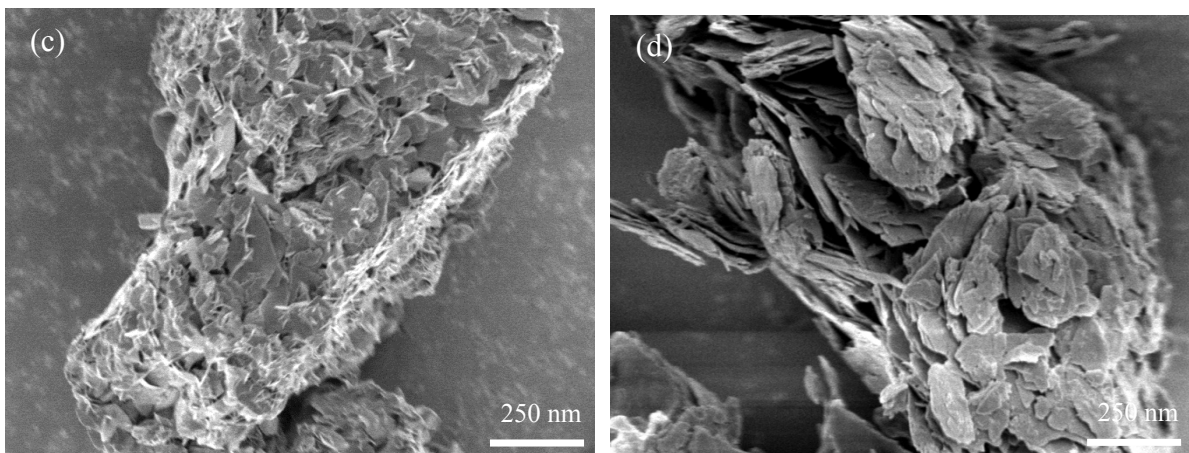
232 like clusters with clearly defined boundaries at a pH of 11.

233

234 The formation of nesquehonite under pH value of 11 was confirmed by the XRD patterns
235 shown in Figure 7. In line with the findings obtained under the $\text{Mg}(\text{OH})_2:\text{CO}_2$ molar ratio of
236 1:1 as revealed in Figure 5, an increase in the pH to 10 and above resulted in the formation of
237 uncarbonated brucite where a flake-like morphology was observed. This “house of cards”
238 texture observed within the prepared samples was attributed to the dissolution-
239 recrystallization-self-assembly growth mechanism as explained in the aforementioned text.
240 The elevated pH used in the experiments conducted in this study increased the solubility of
241 CO_2 in the solution. This has led to a dissolution of the surface of nesquehonite and served as
242 the nucleation points for further hydromagnesite/dypingite plates growing with excessive CO_2
243 at the surface.

244





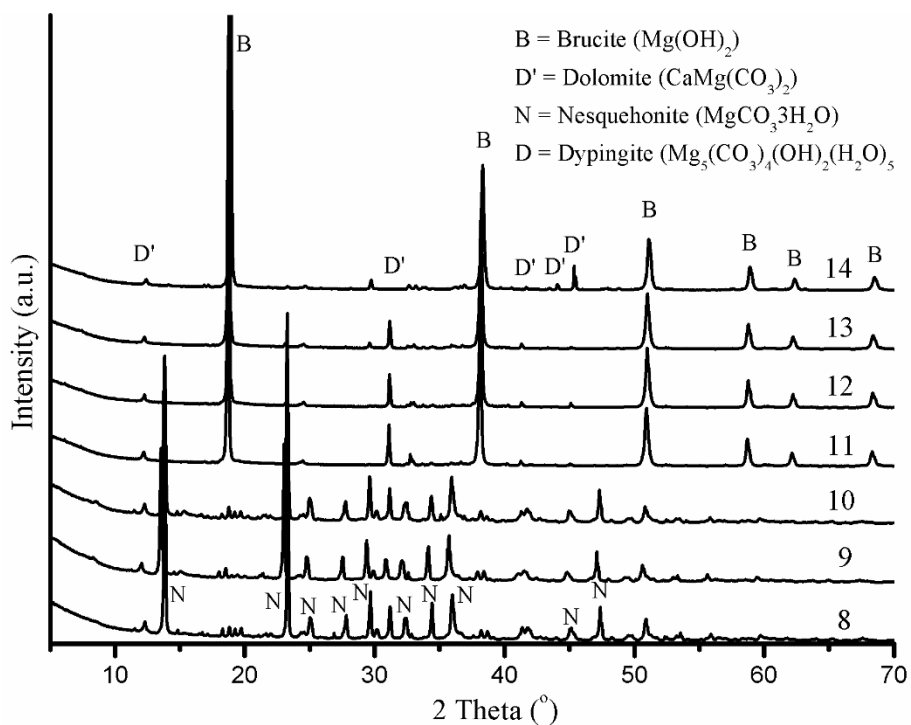
246

247 Figure 6 Typical FESEM images of HMCs obtained at a $\text{Mg}(\text{OH})_2:\text{CO}_2$ molar ratio of 1:2

248

under different pH values of (a) 8, (b) 9, (c) 10 and (d) 11

249



250

251 Figure 7 XRD diffractograms of HMCs obtained at the $\text{Mg}(\text{OH})_2:\text{CO}_2$ molar ratio of 1:2

252

under different pH values

253

254 3.2. Comparison of HMCs synthesized from different source

255 This section aims to provide a comparison of HMCs obtained via reject brine to those of

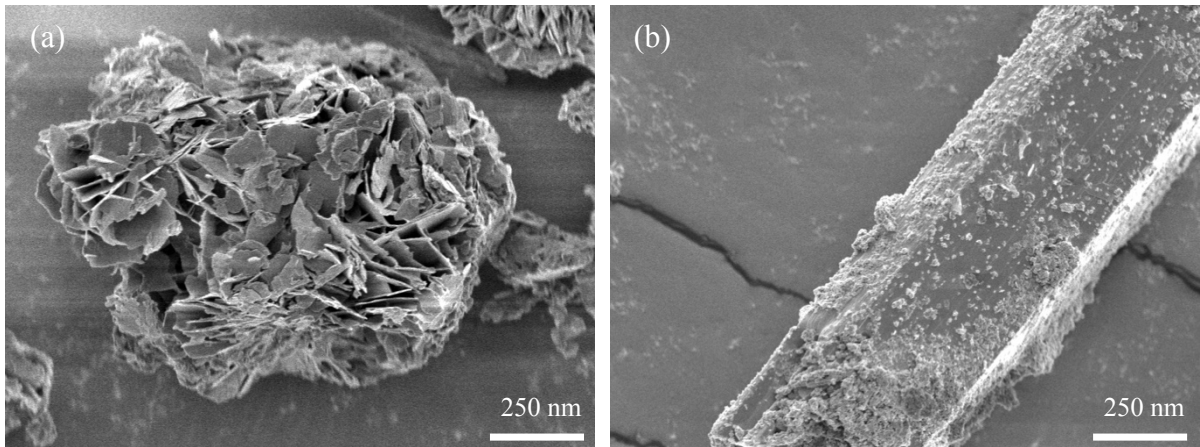
256 chemical Mg(OH)₂ slurry, whose detailed characterization was presented earlier in Section 3.1.
257 The findings presented here aim to use reject brine for the long-term storage of anthropogenic
258 CO₂.

259

260 **3.2.1. Microstructure of HMCs**

261 Figure 8 provides a comparison of the morphologies of HMCs synthesized from Mg(OH)₂
262 slurry and reject brine under a constant pH and Mg(OH)₂:CO₂ molar ratio of 8 and 1:1,
263 respectively. As shown in Figure 8(a), the carbonate crystals obtained via the use of Mg(OH)₂
264 slurry led to a rosette-like morphology. Alternatively, the carbonation of reject brine led to the
265 formation of a needle-like morphology with clear boundaries, as seen in Figure 8(b). The
266 compositions of these rosette- and needle-like particles were confirmed to be nesquehonite and
267 dypingite by XRD patterns revealed in Figure 9, respectively. The formation of different Mg-
268 carbonate phases via the two sources could be associated with the relatively higher reactivity
269 of Mg(OH)₂ prepared from reject brine when compared to that of Mg(OH)₂ slurry (i.e. with a
270 specific surface area of 7.4 vs. 4.8 m²/g as tested by BET analysis). The carbonation of
271 Mg(OH)₂ with a higher reactivity could have capture more CO₂ and enabled the formation of
272 nesquehonite as opposed to dypingite since nesquehonite requires a higher Mg:CO₂ molar ratio
273 as explained in the aforementioned text. This difference in the reactivity of the two samples
274 was also reflected by the absence of the residual brucite peaks in reject brine, as opposed to the
275 clearly defined uncarbonated brucite peaks observed in the Mg(OH)₂ slurry, as seen in Figure
276 9.

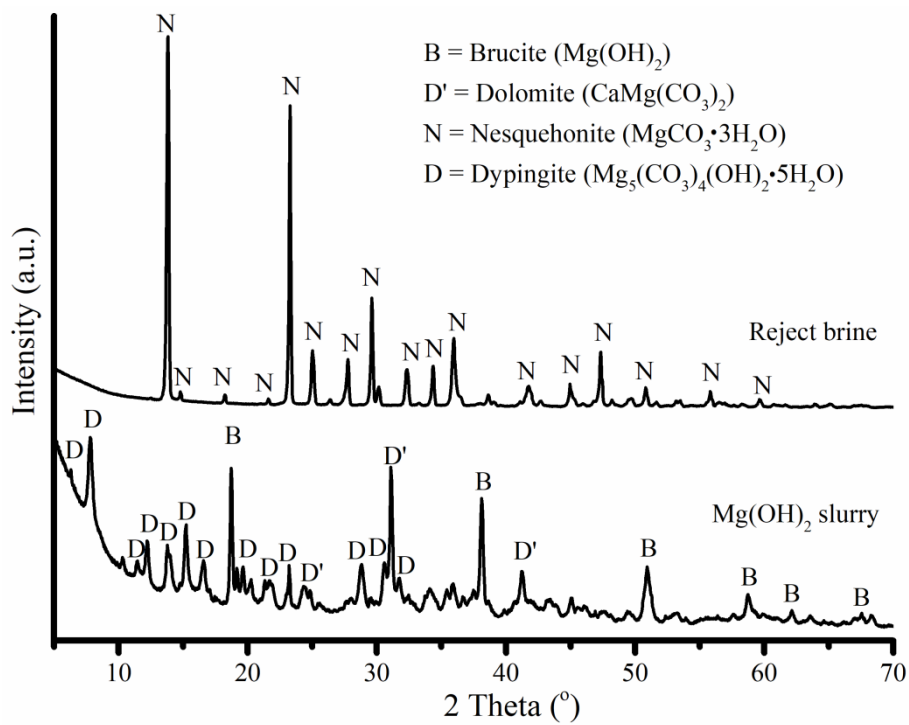
277



278

279 Figure 8 SEM images of HMCs obtained at the $\text{Mg}(\text{OH})_2:\text{CO}_2$ molar ratio of 1:1 under a pH
 280 of 8, showing (a) $\text{Mg}(\text{OH})_2$ slurry and (b) reject brine

281



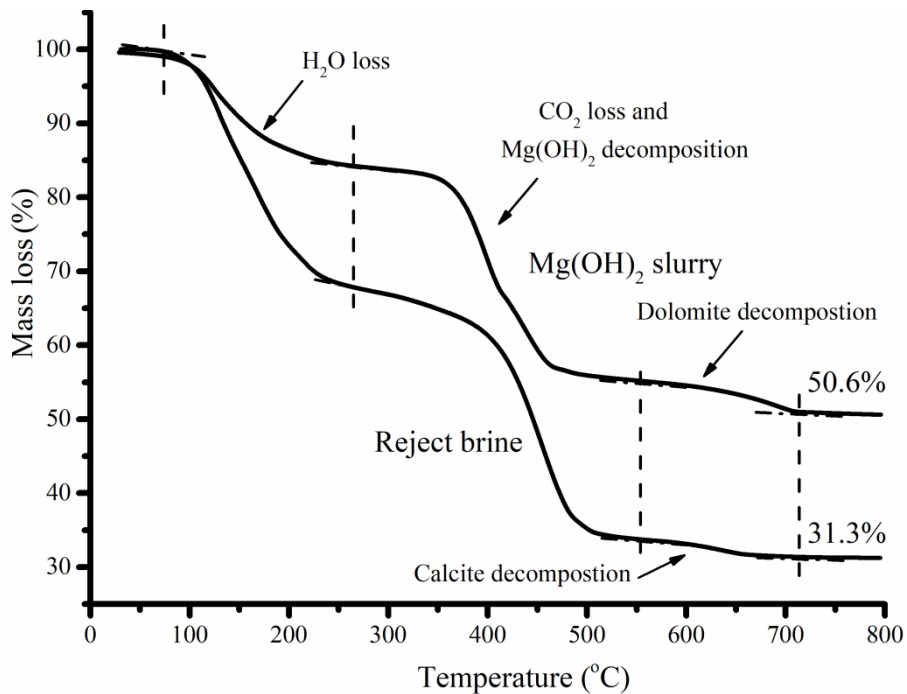
282

283 Figure 9 XRD diffractograms of HMCs obtained from $\text{Mg}(\text{OH})_2$ slurry and reject brine at the
 284 $\text{Mg}(\text{OH})_2:\text{CO}_2$ molar ratio of 1:1 under a pH of 8

285

286 **3.2.2. CO_2 capture and storage**

287 The quantitative analysis of the chemical composition of HMCs and amount of CO₂ used in
 288 their formation was carried out via TG/DTA and ICP-OES analyses. Figure 10 presents the
 289 TG/DTA graphs of HMCs obtained from Mg(OH)₂ slurry and reject brine at the Mg(OH)₂:CO₂
 290 molar ratio of 1:1 and under a pH 8. Both systems demonstrated a similar trend with three
 291 stages of mass loss, which corresponded well with previous studies [36, 54, 55]. Firstly, the
 292 dehydration of HMCs took place at ~100-250 °C, resulting in the loss of H₂O. The second mass
 293 loss occurred between 250 and 550 °C, which was because of the decomposition of
 294 uncarbonated Mg(OH)₂ into MgO as well as the decarbonation of HMCs, resulting in a loss of
 295 H₂O and CO₂. The final mass loss observed between 550 and 700 °C was due to the
 296 decomposition of dolomite and calcite, respectively, which was present as an impurity in the
 297 two systems (i.e. in the form of dolomite in Mg(OH)₂ slurry and calcite in reject brine).
 298



299
 300 Figure 10 Typical TG/DTA curves of HMCs obtained from Mg(OH)₂ slurry and reject brine
 301 at the Mg(OH)₂:CO₂ molar ratio of 1:1 under a pH of 8
 302

303 The chemical composition of the final product was determined via a combination of the results
 304 generated by TG/DTA and ICP-OES, where the recovery rate of Mg^{2+} was measured via ICP-
 305 OES and TG/DTA was used to determine the quantity of each phase derived from XRD results.
 306 Table 2 revealed the composition of the precipitate synthesized via the carbonation of $Mg(OH)_2$
 307 slurry to be composed of 62.1% dypingite and 30.5% uncarbonated brucite. On the other hand,
 308 the carbonation of reject brine led to a precipitate composed of 93.1% nesquehonite and 3.7%
 309 uncarbonated brucite, as detailed in Table 2. These results were used in the calculation of the
 310 percentage of captured CO_2 , which was derived by measuring the mass of CO_2 in the HMCs
 311 (i.e. dypingite/nesquehonite) divided by the initial input of CO_2 degassed to the system at the
 312 $Mg(OH)_2:CO_2$ molar ratio of 1:1. The outcome of these analyses indicated that 43.7% CO_2
 313 could be sequestered in the form of dypingite via the defusing CO_2 into $Mg(OH)_2$ slurry, while
 314 the corresponding ratio of CO_2 sequestered in reject brine was calculated to be 82.6%. The
 315 higher efficiency of CO_2 sequestration achieved via the use of reject brine was associated with
 316 the increased reactivity of $Mg(OH)_2$ synthesized from reject brine. Details of the chemical
 317 composition and the percentage of captured CO_2 were included in the Appendix section.

318

319 Table 2 Chemical composition of HMCs synthesized from $Mg(OH)_2$ slurry and reject brine at
 320 the $Mg(OH)_2:CO_2$ molar ratio of 1:1 under a pH of 8

$Mg(OH)_2$ slurry	Mass (g)	Mass (%)	Reject brine	Mass (g)	Mass (%)
Dypingite	0.6	62.1	Nesquehonite	1.51	93.1
Brucite	0.07	30.5	Brucite	0.06	3.7
Dolomite	0.3	7.4	Calcite	0.05	3.2
CO_2 captured (%)	43.7		CO_2 captured (%)	82.6	

321

322 According to the Paris Agreement, it aims to reduce GHG emissions by 20% (i.e., 7 gigatonnes
 323 CO_2 emission reduction as annual anthropogenic CO_2 emissions is about 35 gigatonnes [56])
 324 in order to hold the increase in the global average temperature to below 2°C above pre-

325 industrial levels [56]. According to the International Desalination Association, the global daily
326 production of desalinated water generated by 18,426 desalination plants worldwide exceeds
327 86.8 million m³ [47]. It is estimated that an equivalent amount of reject brine is generated [47].
328 The concentration of Mg²⁺ in reject brine is around 1700 ppm, and thus around 54 million
329 tonnes of Mg could be recovered every year. With a carbon capture and storage rate of 82.6%
330 in the current study, around 45 million tonnes of CO₂ can be sequestered annually. The
331 suggested methodology thus contributes to around 1% of the required CO₂ emission reduction
332 (*i.e.*, 7 gigatonnes) aimed in the Paris Agreement.

333

334 **4. Summary and Conclusions**

335 This study presented the influences of key parameters including the Mg(OH)₂:CO₂ molar ratio,
336 pH, and Mg(OH)₂ source on the synthesis of HMCs through the carbonation of Mg(OH)₂ slurry.
337 The resulting HMCs were characterized via a combination of techniques including XRD,
338 FESEM, and TG/DTA. Main conclusions drawn from this study are summarized below.

- 339 • The carbonation of Mg(OH)₂ slurry under the elevated of Mg(OH)₂:CO₂ molar ratio
340 resulted in the transformation of dypingite to nesquehonite.
- 341 • Increasing the pH from 8 to 10 was found to promote the carbonation process of
342 Mg(OH)₂, resulting in a higher carbonation degree.
- 343 • A specific “house of cards” texture, involving the formation of rosette-like dypingite
344 flakes on the surface of nesquehonite needles, was discovered under elevated pH and
345 Mg(OH)₂:CO₂ ratios conditions. The formation of this structure was associated with to
346 a dissolution-recrystallization-self-assembly growth mechanism as nesquehonite was
347 seen as a precursor for the further nucleation and seeding of hydromagnesite/dypingite
348 on the surface.

- 349 • Carbonation of $\text{Mg}(\text{OH})_2$ slurry synthesized from reject brine led to high yield, high
350 purity, and high carbonation degree (82.6%) HMCs. Reject brine shows high potential
351 to be used for capture and long-term storage of CO_2 in the form of HMCs.

352

353 The use of compressed commercial CO_2 in the research was to provide a pure source to evaluate
354 CO_2 sequestration rate of the synthesized $\text{Mg}(\text{OH})_2$ from desalination reject brine, which
355 served as a model case study. In the ‘real world’ case, different CO_2 sources and collecting
356 methods such as CO_2 generated from factories, coal burning power plants, and municipal solid
357 waste incineration plants, may be used. However, further study is necessary to evaluate CO_2
358 sequestration efficiency of the synthesized $\text{Mg}(\text{OH})_2$ with different CO_2 sources and collecting
359 methods. Furthermore, it is necessary to evaluate the mass, energy, reagents, wastes that
360 come into play in the global process from the life cycle and life cycle cost viewpoint of HMCs
361 synthesized from reject brine.

362

363 **Acknowledgement**

364

365 The authors would like to acknowledge the financial support from the Singapore Ministry of
366 Education Academic Research Fund Tier 2 (MOE2017-T2-1-087 (S)) for the completion of
367 this research project.

368

369 **References**

370 [1] International Energy Agency, Tracking industrial energy efficiency and CO_2 emissions,
371 in, Organisation for Economic Co-operation and Development, 2007.

- 372 [2] V. Mashayekhizadeh, M.H. Ghazanfari, R. Kharrat, M. Dejam, Pore-level observation of
373 free gravity drainage of oil in fractured porous media, *Transport in porous media*, 87
374 (2011) 561-584.
- 375 [3] M. Dejam, M.H. Ghazanfari, V. Mashayekhizadeh, M. Kamyab, Factors affecting the
376 gravity drainage mechanism from a single matrix block in naturally fractured reservoirs,
377 *Special Topics & Reviews in Porous Media: An International Journal*, 2 (2011).
- 378 [4] M. Dejam, M.H. Ghazanfari, M. Kamyab, M. Masihi, The gas-oil gravity drainage model
379 in a single matrix block: a new relationship between relative permeability and capillary
380 pressure functions, *Journal of Porous Media*, 14 (2011).
- 381 [5] V. Mashayekhizadeh, R. Kharrat, M. Ghazanfari, M. Dejam, An experimental
382 investigation of fracture tilt angle effects on frequency and stability of liquid bridges in
383 fractured porous media, *Petroleum Science and Technology*, 30 (2012) 807-816.
- 384 [6] M. Dejam, H. Hassanzadeh, Z. Chen, Semi-analytical solutions for a partially penetrated
385 well with wellbore storage and skin effects in a double-porosity system with a gas cap,
386 *Transport in porous media*, 100 (2013) 159-192.
- 387 [7] J.D. Figueroa, T. Fout, S. Plasynski, H. McIlvried, R.D. Srivastava, Advances in CO₂
388 capture technology - the US department of energy's carbon sequestration program, *Int. J.*
389 *Greenh. Gas Control*, 2 (2008) 9-20.
- 390 [8] T. Morita, J. Robinson, A. Adegbulugbe, J. Alcamo, D. Herbert, E.L. La Rovere, N.
391 Nakicenovic, H. Pitcher, P. Raskin, K. Riahi, Greenhouse gas emission mitigation
392 scenarios and implications, *Climate Change*, (2001) 115-166.
- 393 [9] P. Forster, V. Ramaswamy, P. Artaxo, T. Berntsen, R. Betts, D.W. Fahey, J. Haywood, J.
394 Lean, D.C. Lowe, G. Myhre, Changes in atmospheric constituents and in radiative
395 forcing. Chapter 2, *Climate Change 2007. The Physical Science Basis*, (2007).

- 396 [10] H. Arakawa, M. Aresta, J.N. Armor, M.A. Barteau, E.J. Beckman, A.T. Bell, J.E.
397 Bercaw, C. Creutz, E. Dinjus, D.A. Dixon, K. Domen, D.L. DuBois, J. Eckert, E. Fujita,
398 D.H. Gibson, W.A. Goddard, D.W. Goodman, J. Keller, G.J. Kubas, H.H. Kung, J.E.
399 Lyons, L.E. Manzer, T.J. Marks, K. Morokuma, K.M. Nicholas, R. Periana, L. Que, J.
400 Rostrup-Nielson, W.M.H. Sachtler, L.D. Schmidt, A. Sen, G.A. Somorjai, P.C. Stair,
401 B.R. Stults, W. Tumas, Catalysis research of relevance to carbon management: Progress,
402 challenges, and opportunities, *Chemical Reviews*, 101 (2001) 953-996.
- 403 [11] R. Lal, Soil carbon sequestration impacts on global climate change and food security,
404 *Science*, 304 (2004) 1623-1627.
- 405 [12] R.S. Haszeldine, Carbon capture and storage: How green can black be?, *Science*, 325
406 (2009) 1647-1652.
- 407 [13] A.B. Rao, E.S. Rubin, A technical, economic, and environmental assessment of amine-
408 based CO₂ capture technology for power plant greenhouse gas control, *Environmental*
409 *Science & Technology*, 36 (2002) 4467-4475.
- 410 [14] H.J. Herzog, CO₂ capture, reuse, and sequestration technologies for mitigating global
411 climate change, in, USDOE Federal Energy Technology Center, Morgantown, WV
412 (United States), 1998.
- 413 [15] A. Botha, C.A. Strydom, Preparation of a magnesium hydroxy carbonate from
414 magnesium hydroxide, *Hydrometallurgy*, 62 (2001) 175-183.
- 415 [16] E. Rendek, G. Ducom, P. Germain, Carbon dioxide sequestration in municipal solid
416 waste incinerator (MSWI) bottom ash, *Journal of Hazardous Materials*, 128 (2006) 73-
417 79.
- 418 [17] J.T. Klopogge, W.N. Martens, L. Nothdurft, L.V. Duong, G.E. Webb, Low temperature
419 synthesis and characterization of nesquehonite, *J. Mater. Sci. Lett.*, 22 (2003) 825-829.

- 420 [18] V. Ferrini, C. De Vito, S. Mignardi, Synthesis of nesquehonite by reaction of gaseous
421 CO₂ with Mg chloride solution: Its potential role in the sequestration of carbon dioxide,
422 Journal of Hazardous Materials, 168 (2009) 832-837.
- 423 [19] E.H. Oelkers, S.R. Gislason, J. Matter, Mineral carbonation of CO₂, Elements, 4 (2008)
424 333-337.
- 425 [20] S.J. Gerdemann, W.K. O'Connor, D.C. Dahlin, L.R. Penner, H. Rush, Ex situ aqueous
426 mineral carbonation, Environmental Science & Technology, 41 (2007) 2587-2593.
- 427 [21] W.J.J. Huijgen, G.J. Witkamp, R.N.J. Comans, Mineral CO₂ sequestration by steel slag
428 carbonation, Environmental Science & Technology, 39 (2005) 9676-9682.
- 429 [22] M. Dejam, H. Hassanzadeh, The role of natural fractures of finite double-porosity
430 aquifers on diffusive leakage of brine during geological storage of CO₂, Int. J. Greenh.
431 Gas Control, 78 (2018) 177-197.
- 432 [23] M. Dejam, H. Hassanzadeh, Diffusive leakage of brine from aquifers during CO₂
433 geological storage, Advances in Water Resources, 111 (2018) 36-57.
- 434 [24] M. Hanchen, V. Prigiobbe, R. Baciocchi, M. Mazzotti, Precipitation in the Mg-carbonate
435 system - effects of temperature and CO₂ pressure, Chemical Engineering Science, 63
436 (2008) 1012-1028.
- 437 [25] W.K. O'Connor, D.C. Dahlin, G.E. Rush, C.L. Dahlin, W.K. Collins, Carbon dioxide
438 sequestration by direct mineral carbonation: process mineralogy of feed and products,
439 Minerals & Metallurgical Processing, 19 (2002) 95-101.
- 440 [26] M.M. Maroto-Valer, D.J. Fauth, M.E. Kuchta, Y. Zhang, J.M. Andrésen, Activation of
441 magnesium rich minerals as carbonation feedstock materials for CO₂ sequestration, Fuel
442 Process. Technol., 86 (2005) 1627-1645.

- 443 [27] A. Sanna, M. Uibu, G. Caramanna, R. Kuusik, M.M. Maroto-Valer, A review of mineral
444 carbonation technologies to sequester CO₂, *Chemical Society Reviews*, 43 (2014) 8049-
445 8080.
- 446 [28] C. Unluer, A. Al-Tabbaa, Enhancing the carbonation of MgO cement porous blocks
447 through improved curing conditions, *Cement and Concrete Research*, 59 (2014) 55-65.
- 448 [29] C. Unluer, A. Al-Tabbaa, Impact of hydrated magnesium carbonate additives on the
449 carbonation of reactive MgO cements, *Cement and Concrete Research*, 54 (2013) 87-97.
- 450 [30] M. Liska, A. Al-Tabbaa, K. Carter, J. Fifield, Scaled-up commercial production of
451 reactive magnesia cement pressed masonry units. Part II: Performance, *Proceedings of
452 the Institution of Civil Engineers-Construction Materials*, 165 (2012b) 225-243.
- 453 [31] M. Liska, A. Al-Tabbaa, K. Carter, J. Fifield, Scaled-up commercial production of
454 reactive magnesium cement pressed masonry units. Part I: Production, *Proceedings of
455 the Institution of Civil Engineers-Construction Materials*, 165 (2012a) 211-223.
- 456 [32] A. Al-Tabbaa, Reactive magnesia cement, *Eco-Efficient Concrete*, (2013) 523-543.
- 457 [33] T.J. Wolery, A software package for geochemical modeling of aqueous systems:
458 package overview and installation guide (version 7.0), Lawrence Livermore National
459 Laboratory Livermore, CA, 1992.
- 460 [34] C. Christ, P. Hostetler, Studies in the system MgO-SiO₂-CO₂-H₂O (II); the activity-
461 product constant of magnesite, *American Journal of Science*, 268 (1970) 439-453.
- 462 [35] J. Kittrick, F. Peryea, Determination of the Gibbs free energy of formation of magnesite
463 by solubility methods, *Soil Science Society of America Journal*, 50 (1986) 243-247.
- 464 [36] P. Ballirano, C. De Vito, S. Mignardi, V. Ferrini, Phase transitions in the Mg-CO₂-H₂O
465 system and the thermal decomposition of dypingite, Mg₅(CO₃)₄(OH)₂·5H₂O:
466 Implications for geosequestration of carbon dioxide, *Chemical Geology*, 340 (2013) 59-
467 67.

- 468 [37] S. Teir, S. Eloneva, C.-J. Fogelholm, R. Zevenhoven, Fixation of carbon dioxide by
469 producing hydromagnesite from serpentinite, *Applied Energy*, 86 (2009) 214-218.
- 470 [38] Y. Wang, Z. Li, G.P. Demopoulos, Controlled precipitation of nesquehonite
471 ($\text{MgCO}_3 \cdot 3\text{H}_2\text{O}$) by the reaction of MgCl_2 with $(\text{NH}_4)_2\text{CO}_3$, *Journal of Crystal Growth*,
472 310 (2008) 1220-1227.
- 473 [39] D.K. Panesar, L. Mo, Properties of binary and ternary reactive MgO mortar blends
474 subjected to CO_2 curing, *Cement and Concrete Composites*, 38 (2013) 40-49.
- 475 [40] Z. Zhang, Y. Zheng, Y. Ni, Z. Liu, J. Chen, X. Liang, Temperature-and pH-dependent
476 morphology and FT-IR analysis of magnesium carbonate hydrates, *The Journal of*
477 *Physical Chemistry B*, 110 (2006) 12969-12973.
- 478 [41] L. Hopkinson, P. Kristova, K. Rutt, G. Cressey, Phase transitions in the system MgO-
479 $\text{CO}_2\text{-H}_2\text{O}$ during CO_2 degassing of Mg-bearing solutions, *Geochimica Et*
480 *Cosmochimica Acta*, 76 (2012) 1-13.
- 481 [42] P. Ballirano, C. De Vito, V. Ferrini, S. Mignardi, The thermal behaviour and structural
482 stability of nesquehonite, $\text{MgCO}_3 \cdot 3\text{H}_2\text{O}$, evaluated by in situ laboratory parallel-beam
483 X-ray powder diffraction: New constraints on CO_2 sequestration within minerals,
484 *Journal of Hazardous Materials*, 178 (2010) 522-528.
- 485 [43] S. Adham, A. Hussain, J.M. Matar, R. Dores, A. Janson, Application of Membrane
486 Distillation for desalting brines from thermal desalination plants, *Desalination*, 314
487 (2013) 101-108.
- 488 [44] S. Mignardi, C. De Vito, V. Ferrini, R.F. Martin, The efficiency of CO_2 sequestration
489 via carbonate mineralization with simulated wastewaters of high salinity, *Journal of*
490 *Hazardous Materials*, 191 (2011) 49-55.

- 491 [45] Y. Soong, A.L. Goodman, J.R. McCarthy-Jones, J.P. Baltrus, Experimental and
492 simulation studies on mineral trapping of CO₂ with brine, Energy Conversion and
493 Management, 45 (2004) 1845-1859.
- 494 [46] Y. Soong, D.L. Fauth, B.H. Howard, J.R. Jones, D.K. Harrison, A.L. Goodman, M.L.
495 Gray, E.A. Frommell, CO₂ sequestration with brine solution and fly ashes, Energy
496 Conversion and Management, 47 (2006) 1676-1685.
- 497 [47] M.H. El-Naas, Reject brine management, Desalination, Trends and Technologies, (2011)
498 237-252.
- 499 [48] PUB, Desalinated Water, [https:// www.pub.gov.sg /watersupply /fournationaltaps](https://www.pub.gov.sg/watersupply/fournationaltaps)
500 /desalinatedwater.
- 501 [49] H. Dong, E.-H. Yang, C. Unluer, F. Jin, A. Al-Tabbaa, Investigation of the properties of
502 MgO recovered from reject brine obtained from desalination plants, Journal of Cleaner
503 Production, 196 (2018) 100-108.
- 504 [50] H. Dong, C. Unluer, E.-H. Yang, A. Al-Tabbaa, Recovery of reactive MgO from reject
505 brine via the addition of NaOH, Desalination, 429 (2018) 88-95.
- 506 [51] H. Dong, C. Unluer, E.-H. Yang, A. Al-Tabbaa, Synthesis of reactive MgO from reject
507 brine via the addition of NH₄OH, Hydrometallurgy, 169 (2017) 165-172.
- 508 [52] Z.H. Hao, F.L. Du, Synthesis of basic magnesium carbonate microrods with a "house of
509 cards" surface structure using rod-like particle template, Journal of Physics and
510 Chemistry of Solids, 70 (2009) 401-404.
- 511 [53] D. Wu, B.J. Luo, W. Liu, L.C. Wang, Y. Yao, X.P. Huang, Study on the process
512 optimization for intermediate Magnesium Carbonate Tri-hydrate, Advanced Materials
513 Research, 960 (2014) 199-203.

514 [54] R. Dell, S. Weller, The thermal decomposition of nesquehonite $\text{MgCO}_3 \cdot 3\text{H}_2\text{O}$ and
515 magnesium ammonium carbonate $\text{MgCO}_3 \cdot (\text{NH}_4)_2\text{CO}_3 \cdot 4\text{H}_2\text{O}$, Transactions of the
516 Faraday Society, 55 (1959) 2203-2220.

517 [55] J. Lanas, J.I. Alvarez, Dolomitic lime: thermal decomposition of nesquehonite,
518 Thermochemica Acta, 421 (2004) 123-132.

519 [56] UNFCCC, The Paris Agreement Conference of the parties to the UNFCCC, (2015).

520

521

522

523 **Appendix – Chemical composition of HMCs and CO₂ captured percentage**

524

525 HMCs synthesized from Mg(OH)₂ slurry

526 Initially, 0.82 g Mg(OH)₂ is added into 200 ml distil water at a Mg(OH)₂/CO₂ molar ratio of 1.

527 Assuming a purity of 92% for Mg(OH)₂, the remaining 8% impurity is dolomite which does

528 not react or dissolve in the solution. The final precipitates consist of uncarbonated brucite,

529 dypingite and dolomite as supported by XRD results (Figures 5 and 7), which after calcination

530 decompose into MgO, MgO, and CaO·MgO, respectively. Let x and y denote the weights of

531 the uncarbonated brucite and dypingite, respectively. The weight of dolomite is 0.066 g

532 calculated based on 8% of the initial sample weight (i.e., 0.82 g). Residues after the TG/DTA

533 test is 50.6% (Figure 10). Based on the given information, the following equation can be

534 established.

535
$$\frac{\frac{40}{58}x + \frac{40}{96.8}y + 0.82 \times 0.08 \times \frac{96}{184}}{x + y + 0.82 \times 0.08} = 0.506 \quad (A1)$$

536 Furthermore, the concentration of Mg²⁺ in the residue was measured to be 308.4 ppm (0.308

537 g/L) as shown in Table 3. Thus,

538
$$\frac{\frac{24}{58}x + \frac{24}{96.8}y}{0.2} = \frac{\frac{24}{58} \times 0.82 \times 0.92}{0.2} - 0.308$$

539 (A2)

540

541 By solving the two Eqns. (A1) and (A2), the weights of uncarbonated brucite and dypingite are

542 calculated to be 0.27 g and 0.55 g, respectively. The sum of the weights of uncarbonated brucite,

543 dolomite and dypingite was calculated to be 0.89 g, which was higher than 0.46 g of the

544 weighted precipitate as shown in Table 3. This was mainly due to the weight losses during the

545 process of separating the samples from the solution and grinding. The captured CO₂ percentage

546 was calculated by measuring the weight of CO₂ in the HMCs (dypingite) divided by the initial

547 input of CO₂ degassed to the system at the Mg(OH)₂/CO₂ molar ratio of 1, which was calculated
 548 to be 43.7% in consideration of 8% impurity.

549

550 Table A1 Concentration of Mg²⁺ in the residue and final weight of HMCs obtained from
 551 Mg(OH)₂ slurry and reject brine

	Mg ²⁺ in the residue solution (ppm)	Weight of solids (g)
Mg(OH) ₂ slurry	309.9 ± 5.2	0.46 ± 0.20
Reject brine	161.5 ± 9.1	1.24 ± 0.14

552

553 HMCs synthesized from reject brine

554 The same principal applies to HMCs synthesized from the reject brine. The Mg(OH)₂ sample
 555 precipitated from reject brine in the first step contains 6.3% calcite as the impurity which has
 556 been detailed in [50]. The XRD result confirms that HMCs after carbonation of Mg(OH)₂
 557 consisted of nesquehonite, uncarbonated brucite and calcite, which after calcination decompose
 558 into **MgO, MgO and CaO**, respectively. Let x and y denoted the weights of uncarbonated brucite
 559 and nesquehonite, respectively. The weight of calcite is 0.052 g calculated based on 6.3% of
 560 the initial sample weight (i.e., 0.82 g). Residues after the TG/DTA test is 31.3% (Figure 10).
 561 Based on the given information, the following equation can be established.

$$562 \frac{\frac{40}{58}x + \frac{40}{138}y + 0.82 \times 0.063 \times \frac{56}{100}}{x + y + 0.82 \times 0.063} = 0.313 \quad (A3)$$

563 Furthermore, the concentration of Mg²⁺ in the residue brine was measured to be 159.3 ppm
 564 (0.159 g/L) as shown in Table 3. Thus,

$$565 \frac{\frac{24}{58}x + \frac{24}{138}y}{0.2} = \frac{\frac{24}{58} \times 0.82 \times 0.937}{0.2} - 0.159 \quad (A4)$$

566

567 By solving the two Eqns. (A1) and (A2), the weights of uncarbonated brucite and nesquehonite
 568 are calculated to be 0.06 g and 1.51 g, respectively. The captured CO₂ percentage was
 569 calculated by measuring the weight of CO₂ in the HMCs (nesquehonite) divided by the initial

570 input of CO₂ degassed to the system at the Mg(OH)₂/CO₂ molar ratio of 1, which was calculated
571 to be 82.6% in consideration of 6.3% impurity. A successful sequestration of CO₂ into reject
572 brine as HMCs was therefore achieved to obtain an efficiency as high as 82.6%, which was
573 significantly improved compared to the Mg(OH)₂ slurry.

574

- Carbonation of $\text{Mg}(\text{OH})_2$ slurry obtained from reject brine is studied
- $\text{Mg}(\text{OH})_2:\text{CO}_2$ ratio and pH influence the type and amount of carbonates
- Formation of nesquehonite is observed at high $\text{Mg}(\text{OH})_2:\text{CO}_2$ ratios and pH
- A “house of cards” texture is formed with an increase in pH and $\text{Mg}(\text{OH})_2:\text{CO}_2$ ratio
- Carbonation of $\text{Mg}(\text{OH})_2$ slurry obtained from reject brine has a CCS efficiency of 82.6%

1 **Microstructure and carbon storage capacity of hydrated magnesium carbonates**
2 **synthesized from different sources and conditions**

3
4 Haoliang Dong^a, Cise Unluer^a, En-Hua Yang^{a,*}, Fei Jin^b, Abir Al-Tabbaa^b

5
6 ^a School of Civil and Environmental Engineering, Nanyang Technological University, 50
7 Nanyang Avenue, Singapore 639798, Singapore

8 ^b Department of Engineering, University of Cambridge, Trumpington Street, Cambridge CB2
9 1PZ, UK

10
11 **Abstract**

12 Recently, the mineral carbonation via the reaction of CO₂ with saline aquifers received much
13 attention as one of the most promising ways for geologic CO₂ storage. This paper reports
14 microstructure and carbon storage capacity of hydrated magnesium carbonates (HMCs)
15 synthesized from different sources, *i.e.*, reject brine and commercial Mg(OH)₂ slurry, and under
16 different conditions, *i.e.*, pH (8-14) and Mg(OH)₂:CO₂ molar ratio (1:1-1:7). Results show that
17 dypingite (Mg₅(CO₃)₄(OH)₂·5H₂O) is the main phase forming at lower Mg(OH)₂:CO₂ ratios.
18 An increase in the Mg(OH)₂:CO₂ ratio and/or pH leads to the precipitation of nesquehonite
19 (MgCO₃·3H₂O). A unique “house of cards” texture, involving formation of the rosette-like
20 dypingite flakes on the surface of nesquehonite needles, is discovered under elevated pH and
21 Mg(OH)₂:CO₂ ratios. HMCs synthesized from reject brine exhibit a much higher carbon
22 storage capacity of 82.6% than that produced from the commercial Mg(OH)₂ slurry (43.7%).

* Corresponding author. Address: N1-01b-56, 50 Nanyang Avenue, Singapore 639798. Tel.: +65 6790 5291;
fax: +65 6791 0676. *E-mail*: ehyang@ntu.edu.sg

23 Findings from this study advance understanding of mineral recovery from reject brine and the
24 capture and long-term storage of CO₂ in the form of HMCs.

25

26 **Keywords:** *Reject brine; Mg(OH)₂; pH; hydrated magnesium carbonates (HMCs); carbon*
27 *capture and storage*

28

29 **1. Introduction**

30 Fossil fuels have been the world's primary energy source, providing over 85% of the energy
31 demands worldwide [1-6]. However, nearly 83% of the anthropogenic greenhouse gas (GHG)
32 emissions are coming from combustion and non-fuel uses of fossil fuels [7]. CO₂, which is the
33 main GHG, has caused most of the global warming since it has the highest positive radiative
34 forcing and far more abundant in the atmosphere than other heat-trapping gases [8, 9]. The
35 concentration of CO₂ in the atmosphere has increased ~30% from 325 parts per million (ppm)
36 at the beginning of the industrial era in 1970 to 409.7 ppm in May 2017 measured in Mauna
37 Loa Observatory. Consequently, much attention has been drawn to the carbon management
38 [10-12]. Carbon capture and storage (CCS) provides a feasible way to reduce the build-up of
39 CO₂ in the atmosphere [13, 14]. CCS concept covers broad fields such as ocean, terrestrial,
40 geological, biological and chemical approaches to store CO₂ gas in the long term [15-18],
41 among which mineral carbonation via the reaction of CO₂ with saline aquifers is one of the
42 most promising geologic CO₂ storage options [19-23]. Magnesium-based minerals have
43 attracted great attentions worldwide as they show the potential to sequester anthropogenic
44 CO₂ to counterpart the global warming [24-27]. Furthermore, reactive magnesia (MgO) cement
45 has been studied as a potential alternative to the Portland cement due to its ability to sequester
46 significant amount of carbon dioxide (CO₂) and potential to be fully recycled [28-32].

47

48 Although the most thermodynamically stable carbonate for magnesium is in the anhydrous
49 form, *i.e.*, magnesite (MgCO_3) [33-35], formation of magnesite at the ambient condition is not
50 common. Instead, formation of hydrated magnesium carbonates (HMCs) prevails as Mg^{2+} ions
51 in the solution are highly hydrated [24]. HMCs are a class of magnesium compounds that form
52 in $\text{MgO-CO}_2\text{-H}_2\text{O}$ systems, where the carbonation of magnesium systems generate a variety of
53 phases, including dypingite ($\text{Mg}_5(\text{CO}_3)_4(\text{OH})_2 \cdot 5\text{H}_2\text{O}$) [36], hydromagnesite
54 ($\text{Mg}_5(\text{CO}_3)_4(\text{OH})_2 \cdot 4\text{H}_2\text{O}$) [37], and nesquehonite ($\text{MgCO}_3 \cdot 3\text{H}_2\text{O}$) [18, 38]. It has been reported
55 that inclusion of HMCs in reactive MgO cement enhances carbonation of the resulting binder
56 [39].

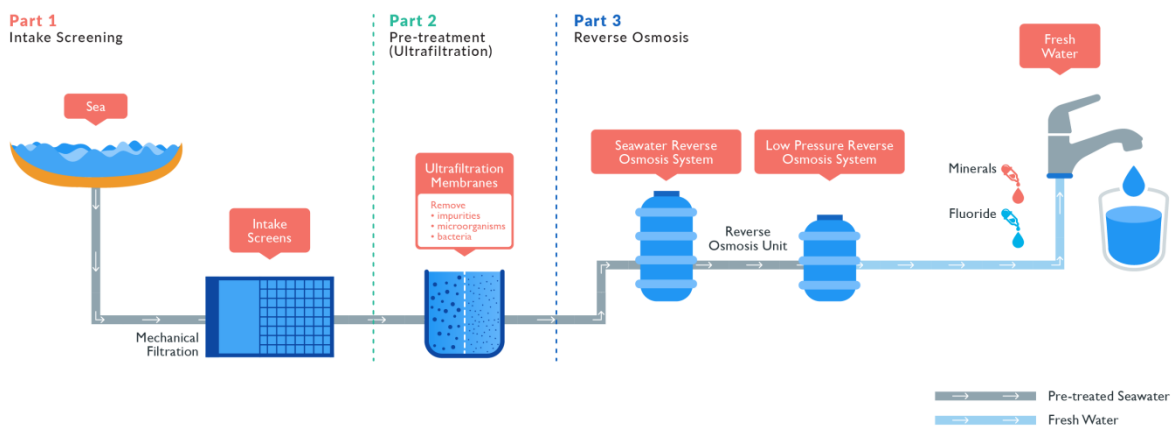
57
58 Theoretically, the formation of different phases of HMCs with different morphologies is
59 influenced by temperature, pH and CO_2 partial pressure [24, 40, 41]. Recent experimental
60 studies show that the precipitation of nesquehonite with needle-like morphology in an aqueous
61 solution occurs commonly under ambient conditions [15, 18, 38]. As the reaction temperatures
62 (333-368 K) and pH values increased, needle-like nesquehonite was replaced by
63 hydromagnesite with sheet-like morphology since nesquehonite is widely known to transform
64 to hydromagnesite at temperature above 50°C [40]. Hydromagnesite was reported to form at
65 120°C and P_{CO_2} of 3 bar, which gradually transformed to magnesite within 5-15 hours.
66 However, a further increase of P_{CO_2} to 100 bar at 120°C resulted in the direct precipitation of
67 magnesite [24]. The thermal behavior of the synthesized HMCs (*e.g.*, nesquehonite) has been
68 tested through real time in-situ X-ray diffraction (XRD), which indicated that nesquehonite and
69 dypingite remained thermal and structural stable up to 373 K and 435 K, respectively [36, 42].
70 Under the continued thermal treatment, nesquehonite transited into magnesite which was even
71 thermally stable up to 600 K, while dypingite transited into hydromagnesite at around 570 K,
72 assuring the long-term storage of CO_2 . However, the influences of $\text{Mg}(\text{OH})_2/\text{CO}_2$ molar ratios

73 and pH on the phases, morphology, and CCS efficiency of HMCs have yet been studied
74 systematically.

75

76 Desalination is a process that removes minerals from saline water. In coastal regions such as
77 Singapore where sources of fresh water are limited, desalination provides a feasible option to
78 produce fresh water. However, a high salty waste stream (*i.e.*, reject brine) would be generated
79 as much as the produced desalinated water at the end of the process [43]. Reject brine is a much
80 more complex media because chemicals are often added into the intake seawater (*e.g.*, to
81 precipitate the colloidal particles before running through the ultra-filtration) in the desalination
82 process (Fig. 1). Although many studies have investigated mineral trapping of CO₂ into saline
83 aquifers (*e.g.*, seawater, natural brine, or synthesized MgCl₂ solution) [18, 36, 42, 44-46], very
84 few has reported the use of reject brine as the CO₂ reservoir [47] and no study has proposed to
85 use reject brine as the Mg(OH)₂ source to synthesize HMCs.

86



87

88 Figure 1 Schematic illustration of the typical process in a reverse osmosis desalination plant

89

[48]

90

91 In this paper, influence of key parameters including $\text{Mg}(\text{OH})_2:\text{CO}_2$ molar ratio, pH, and
92 $\text{Mg}(\text{OH})_2$ source on HMCs synthesis were investigated. The resulting HMCs were
93 characterized by means of XRD, scanning electron microscopy (SEM), and
94 thermogravimetric/differential thermal analysis (TG/DTA) to reveal phases, morphology, and
95 CCS efficiency of HMCs synthesized under different conditions. In the following sections,
96 materials and methodologies are presented first, followed by results presentation and
97 discussion.

98

99 **2. Materials and Methodology**

100 **2.1. Materials**

101 Reject brine sample was collected from a local desalination plant which generates 318,500 m³
102 desalinated water per day. The sample was filtrated through a 45 μm membrane filter to remove
103 suspended solids before further analysis. An inductively coupled plasma-optical emission
104 spectroscopy (ICP-OES) was used to analyze the chemical composition of reject brine in the
105 current study (Table 1). Analytical grade $\text{Mg}(\text{OH})_2$ (92% pure) and analytical grade sodium
106 hydroxide (NaOH) with a purity of 97% were both purchased from VWR Pte Ltd in Singapore.
107 Compressed CO_2 was purchased from Leeden National Oxygen Ltd in Singapore.

108

109 Table 1 Chemical composition of reject brine

Element	Cl	Na	SO_4	Mg	K	Ca	Sr	B	Si	Li	P	Al
Concentration (ppm)	65593	13580	4323	1718	846	471	14.6	3.8	3.7	0.3	0.2	0.1

110

111 **2.2. Methodology**

112 In the first approach, 0.82 g commercially available analytical grade $\text{Mg}(\text{OH})_2$ was dissolved
113 into 200 ml ultra-pure water to prepare the $\text{Mg}(\text{OH})_2$ slurry. To study the influences of

114 $\text{Mg(OH)}_2/\text{CO}_2$ molar ratios and pH on the microstructures of HMCs , three sets of experiments
115 were designed at controlled conditions, *i.e.*, $\text{Mg(OH)}_2:\text{CO}_2$ molar ratio (1:1-1:7) and pH (8-14).
116 CO_2 was sparged into the slurry at a rate of 100 ml/min at room temperature under pre-
117 determined conditions as follows,

118 a) pH = 8, $\text{Mg(OH)}_2:\text{CO}_2$ molar ratio = 1:1 to 1:7

119 b) pH = 8 to 11, $\text{Mg(OH)}_2:\text{CO}_2$ molar ratio = 1:1

120 c) pH = 8 to 11, $\text{Mg(OH)}_2:\text{CO}_2$ molar ratio = 1:2

121

122 In the second approach, Mg(OH)_2 was first synthesized from the reject brine via the addition
123 of NaOH at an optimized condition (*i.e.*, NaOH/ Mg^{2+} ratio of 2 at 25°C) determined from our
124 previous work [49-51], which results high yield and high purity Mg(OH)_2 . After which, 0.82 g
125 of synthesized Mg(OH)_2 was mixed with 200 ml ultra-pure water. CO_2 was sparged into the
126 slurry at a rate of 100 ml/min at room temperature under controlled condition (*i.e.*, pH = 8,
127 $\text{Mg(OH)}_2:\text{CO}_2$ molar ratio = 1:1).

128

129 A pH/thermometer probe, inserted into reject brine, was used to continuously record the
130 temperature and pH during the experiment. A CO_2 flowmeter was used to monitor and record
131 the volume of CO_2 diffused into the slurry. Once the diffused CO_2 reached the pre-determined
132 value (*i.e.*, calculated based on the designed $\text{Mg(OH)}_2:\text{CO}_2$ molar ratio), the reaction was
133 terminated. 1M NaOH was added into the slurry continuously to maintain the pH to the
134 designed value since sparging CO_2 lowered the pH of slurry. HMCs were separated from the
135 solution by a centrifuge and washed three times using ultra-pure water. The washed samples
136 were fully dried in an oven at low temperature (*i.e.*, 40°C) to avoid any phase changes, before
137 being ground into powder form. The prepared powder was finally passed through a 125 μm
138 sieve for further microstructural analysis.

139

140 ICP-OES (PerkinElmer Optima DV2000) was employed to measure the chemical composition
141 of the reject brine before and after the reactions. The XRD (Bruker D8 Advance) diffractograms
142 of the synthesized HMCs were recorded from 5° to 70° at $0.02^\circ/\text{step}$ with a $\text{CuK}\alpha$ radiation at
143 40 kV and 40 mA. The morphology of the synthesized HMCs was investigated by a field
144 emission SEM (JSM-7600F). TG/DTA (PyrisDiamond 4000) of the synthesized HMCs was
145 operated at a heating rate of $10^\circ\text{C}/\text{min}$ under the air flow condition.

146

147 **3. Results and Discussion**

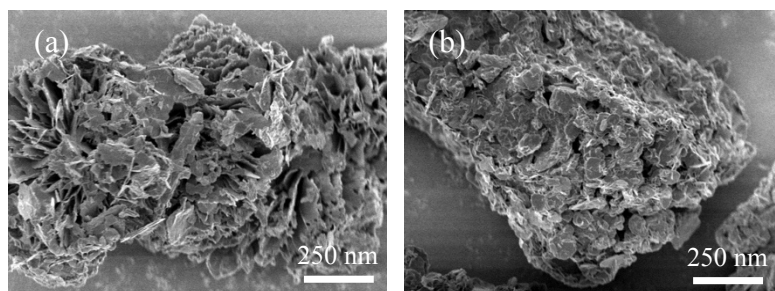
148 **3.1. Characterization of HMCs synthesized from $\text{Mg}(\text{OH})_2$ slurry**

149 **3.1.1. Effect of $\text{Mg}(\text{OH})_2/\text{CO}_2$ molar ratio**

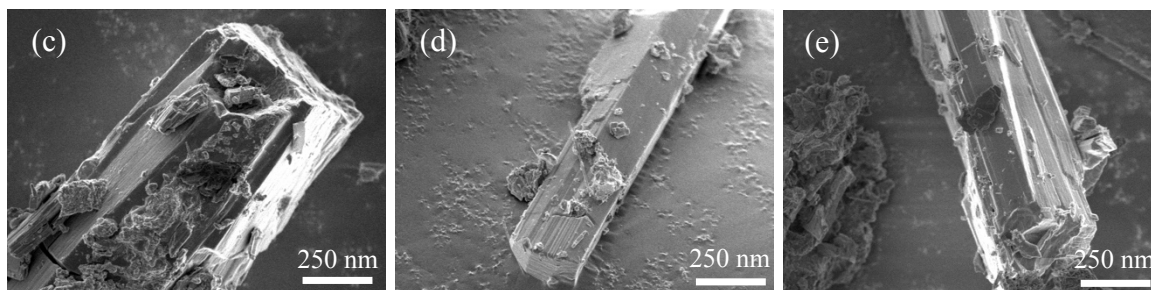
150 Figure 2 shows the FESEM images of all samples obtained under a constant pH of 8 while the
151 $\text{Mg}(\text{OH})_2:\text{CO}_2$ molar ratio was varied between 1:1 and 1:7. The morphologies of the obtained
152 HMCs dramatically changed with the $\text{Mg}(\text{OH})_2:\text{CO}_2$ molar ratio. For instance, the rosette-like
153 morphology observed when the $\text{Mg}(\text{OH})_2:\text{CO}_2$ molar ratio was 1:1 (Fig. 2a), which was
154 eventually replaced by rod-like structures with smooth surfaces when this ratio gradually
155 increased to 1:6 (Figs. 2b-f). The boundaries of these rod-like carbonate phases became clearer
156 with an increase in the $\text{Mg}(\text{OH})_2:\text{CO}_2$ molar ratio. A further increase in the $\text{Mg}(\text{OH})_2:\text{CO}_2$
157 molar ratio to 1:7 revealed the formation of a layer of rosette-like flakes around the original
158 rod-like morphology, producing a “house of cards” texture on the surface [52], as shown in
159 Fig. 2g.

160

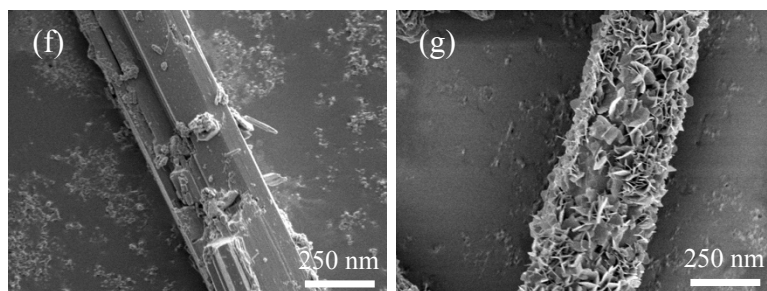
161



162



163



164 Figure 2 FESEM images of HMCs obtained under a pH of 8 at different $\text{Mg}(\text{OH})_2:\text{CO}_2$ molar
165 ratios of (a) 1:1, (b) 1:2, (c) 1:3, (d) 1:4, (e) 1:5, (f) 1:6 and (g) 1:7
166

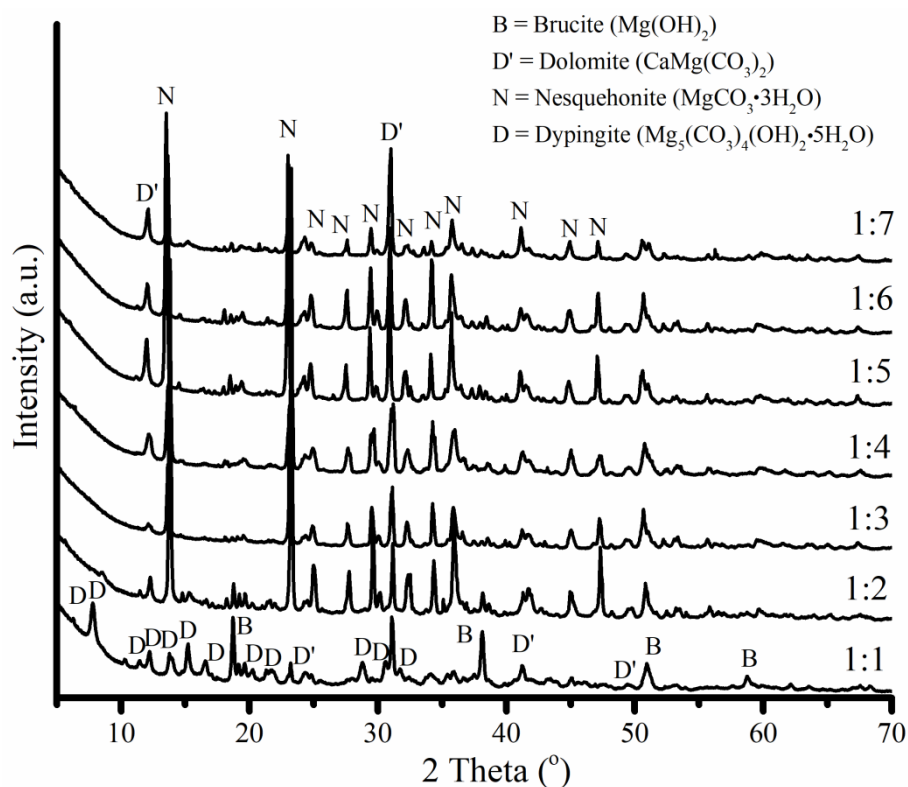
167 Fig. 3 indicates the XRD diffractograms of the same set of samples obtained under a pH of 8
168 at different $\text{Mg}(\text{OH})_2:\text{CO}_2$ molar ratios. The XRD patterns confirmed that the rosette- and rod-
169 like particles observed in Fig. 2 could be attributed to dypingite and nesquehonite, respectively.
170 These morphological observations were in line with the previous literature [18, 36, 41], where
171 the distinct morphologies of dypingite and nesquehonite were reported. At the $\text{Mg}(\text{OH})_2:\text{CO}_2$
172 molar ratio of 1:1, the precipitates consisted of dypingite, uncarbonated brucite and dolomite
173 that was present as an impurity within $\text{Mg}(\text{OH})_2$. An increase in the $\text{Mg}(\text{OH})_2:\text{CO}_2$ molar ratio
174 to 1:2 revealed a reduction in the amount of uncarbonated brucite, resulting in the domination
175 of nesquehonite. These results corresponded well with the chemical composition of different

176 carbonate phases. Accordingly, the abundance of nesquehonite could be associated with the
177 availability of higher amounts of CO₂ introduced into the mix under higher Mg(OH)₂:CO₂
178 molar ratios. This is because nesquehonite (MgCO₃·3H₂O) requires a higher Mg:CO₂ molar
179 ratio of 1:1 than dypingite (Mg₅(CO₃)₄(OH)₂·5(H₂O)), which can theoretically form at a
180 corresponding ratio of 1:0.8. Further increase of the Mg(OH)₂:CO₂ molar ratio from 1:2 to 1:7
181 did not lead to significant changes in the XRD patterns, where nesquehonite continued to be
182 the dominate phase which is consistent with the SEM observation (Fig. 2).

183

184 The “house of cards” morphology is related to a dissolution-recrystallization self-assembly
185 growth mechanism when the dissolution rate of nesquehonite was faster than the precipitation
186 rate of hydromagnesite [52]. Thus, the formation of “house of cards” texture on the surface of
187 HMCs synthesized at Mg(OH)₂:CO₂ molar ratio of 1:7 (Fig. 2g) reveals that while
188 nesquehonite is still the dominating phase of the main body (Fig. 3), nesquehonite on the
189 surface was transformed into hydromagnesite phase due to elevated CO₂ concentration.

190



191

192 Figure 3 XRD diffractograms of HMCs obtained under a pH of 8 at different $\text{Mg}(\text{OH})_2:\text{CO}_2$
 193 molar ratios

194

195 **3.1.2. Effect of pH at $\text{Mg}(\text{OH})_2$ -to- CO_2 molar ratio of 1**

196 Figure 4 illustrates the FESEM images of the samples obtained under different pH values
 197 ranging between 8 and 11, at a constant $\text{Mg}(\text{OH})_2:\text{CO}_2$ molar ratio of 1:1. At the lower pH
 198 values of < 11 , the obtained carbonates displayed rosette-like morphologies with an average
 199 dimension of $\sim 2 \mu\text{m}$, as shown in Figures 4(a)-(c). These rosette-like formations were
 200 confirmed to be dypingite, as shown by the XRD patterns presented in Figure 5. As the pH
 201 increased from 8 to 10, the intensity of the uncarbonated brucite peak revealed a decrease
 202 relative to the others, possibly indicating a reduction in the amount of brucite and an associated
 203 higher degree of carbonation at elevated pH levels. This increase in the carbonation degree
 204 could be associated with the higher $\text{CO}_3^{2-}:\text{HCO}_3^-$ ratios in the prepared solutions at elevated
 205 pH levels. An increase in the pH led to higher concentrations of OH^- , therefore enabling the

206 conversion of HCO_3^- to CO_3^{2-} , which then reacted with Mg^{2+} , leading to the precipitation of
207 higher amounts of HMCs in the solution. Alternatively, a further increase in the pH from 11 to
208 14 lowered the carbonation degree of brucite, which was observed with its flake-like
209 morphology in Figure 4(d). These results were in line with the findings reported in previous
210 studies, where the optimal pH for the carbonation of brucite was shown to be around 9 [53].

211

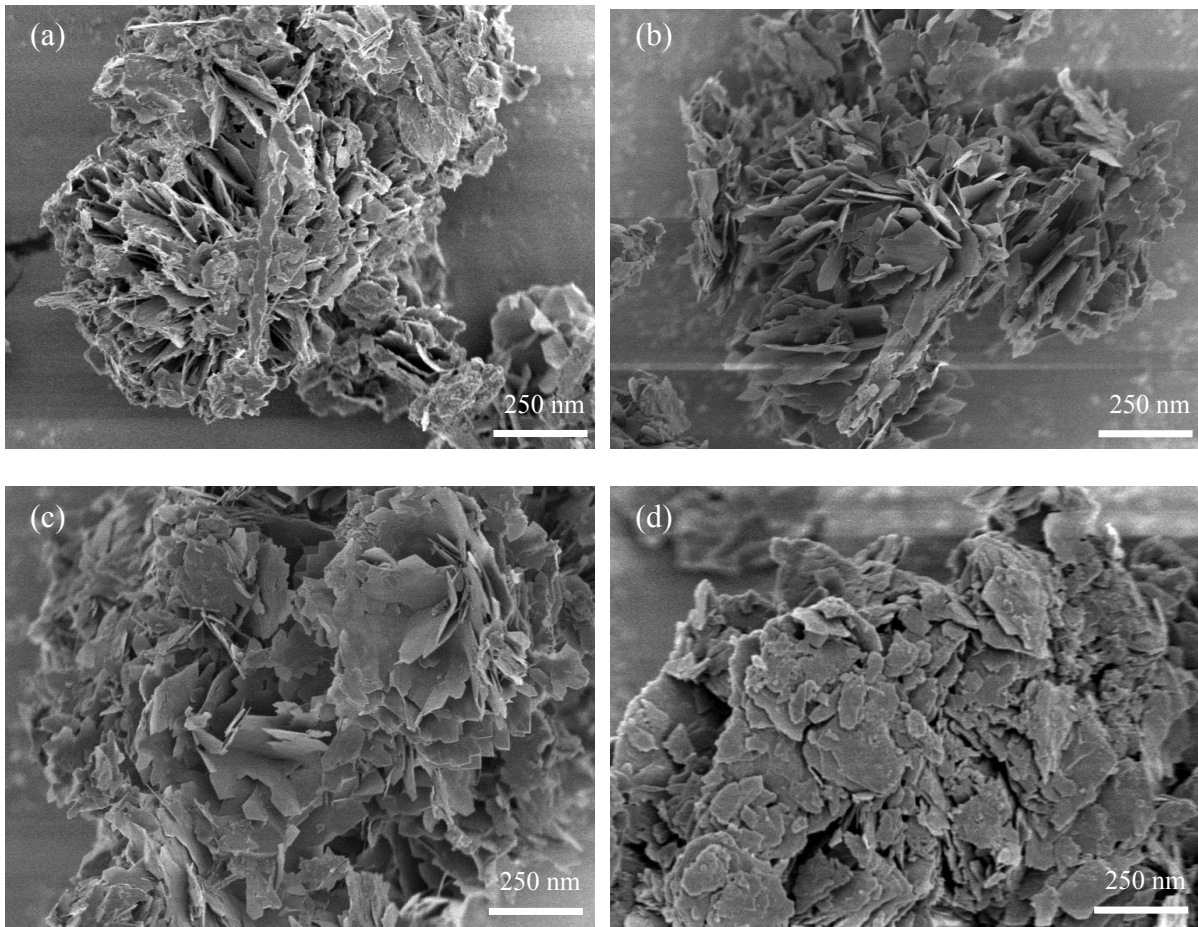
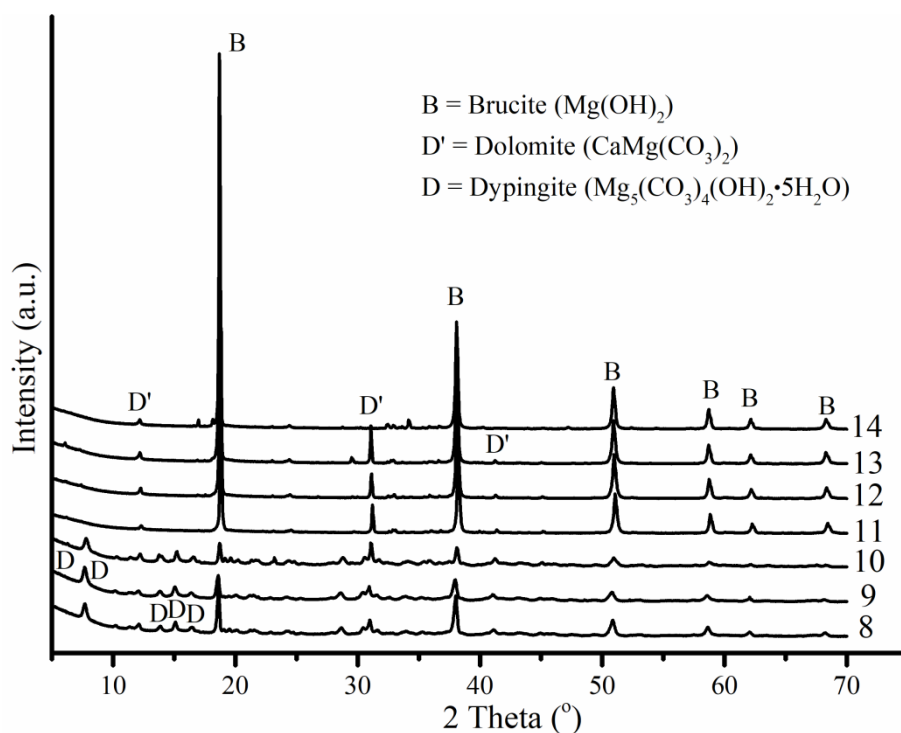


Figure 4 FESEM images of HMCs obtained at the $\text{Mg}(\text{OH})_2:\text{CO}_2$ molar ratio of 1:1 under different pH values of (a) 8, (b) 9, (c) 10 and (d) 11



217

218 Figure 5 XRD diffractograms of HMCs obtained at the $\text{Mg}(\text{OH})_2:\text{CO}_2$ molar ratio of 1:1

219 under different pH values

220

221 3.1.3 Effect of pH at $\text{Mg}(\text{OH})_2:\text{CO}_2$ molar ratio of 1:2

222 Figure 6 displays the morphologies of HMCs obtained under different pH values at the

223 $\text{Mg}(\text{OH})_2:\text{CO}_2$ molar ratio of 1:2. Different from HMCs obtained at the $\text{Mg}(\text{OH})_2:\text{CO}_2$ molar

224 ratio of 1:1, where the presence of dypingite with a rosette-like morphology dominated

225 regardless of the pH value; HMCs obtained at the $\text{Mg}(\text{OH})_2:\text{CO}_2$ molar ratio of 1:2 clearly

226 demonstrated a different morphology. Instead of the previously observed rosette-like plates, a

227 rod-like structure presenting the “house of cards” texture was seen in samples obtained under

228 pH values of 8 and 9 (Figs. 6a-b). An increase in the pH from 8 onwards resulted in the

229 distortion of the originally clear borders of the nesquehonite crystals, whose shape transformed

230 from the rod-like structure to a cluster of flakes forming on top. This change was mostly

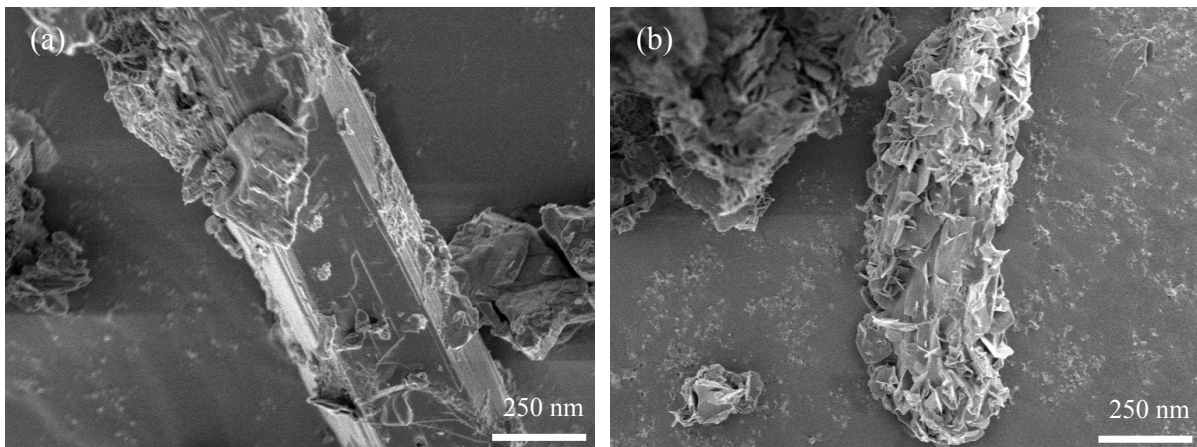
231 obvious at pH values of 10 and 11 (Figures 6(c) and (d)), which revealed the formation of flake-

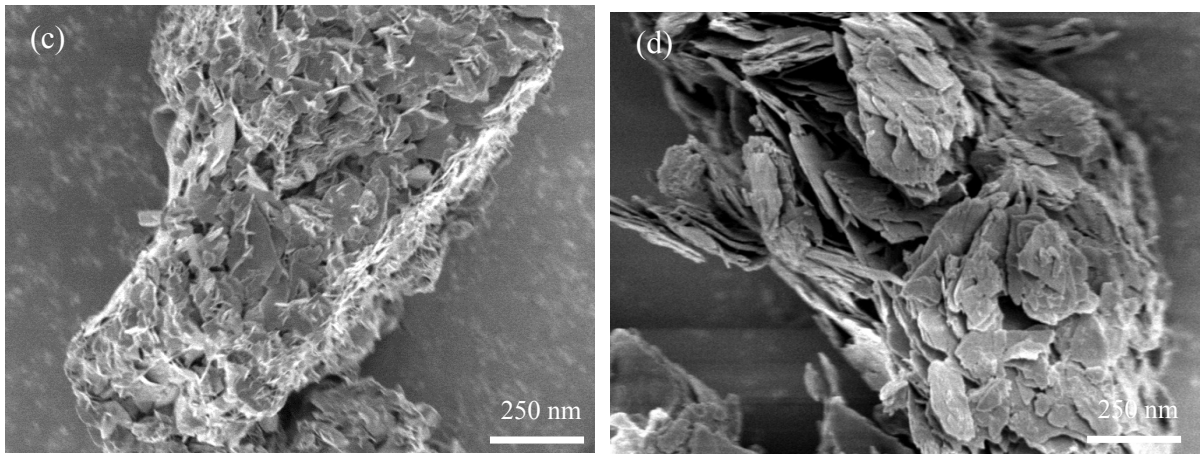
232 like clusters with clearly defined boundaries at a pH of 11.

233

234 The formation of nesquehonite under pH value of 11 was confirmed by the XRD patterns
235 shown in Figure 7. In line with the findings obtained under the $\text{Mg}(\text{OH})_2:\text{CO}_2$ molar ratio of
236 1:1 as revealed in Figure 5, an increase in the pH to 10 and above resulted in the formation of
237 uncarbonated brucite where a flake-like morphology was observed. This “house of cards”
238 texture observed within the prepared samples was attributed to the dissolution-
239 recrystallization-self-assembly growth mechanism as explained in the aforementioned text.
240 The elevated pH used in the experiments conducted in this study increased the solubility of
241 CO_2 in the solution. This has led to a dissolution of the surface of nesquehonite and served as
242 the nucleation points for further hydromagnesite/dypingite plates growing with excessive CO_2
243 at the surface.

244





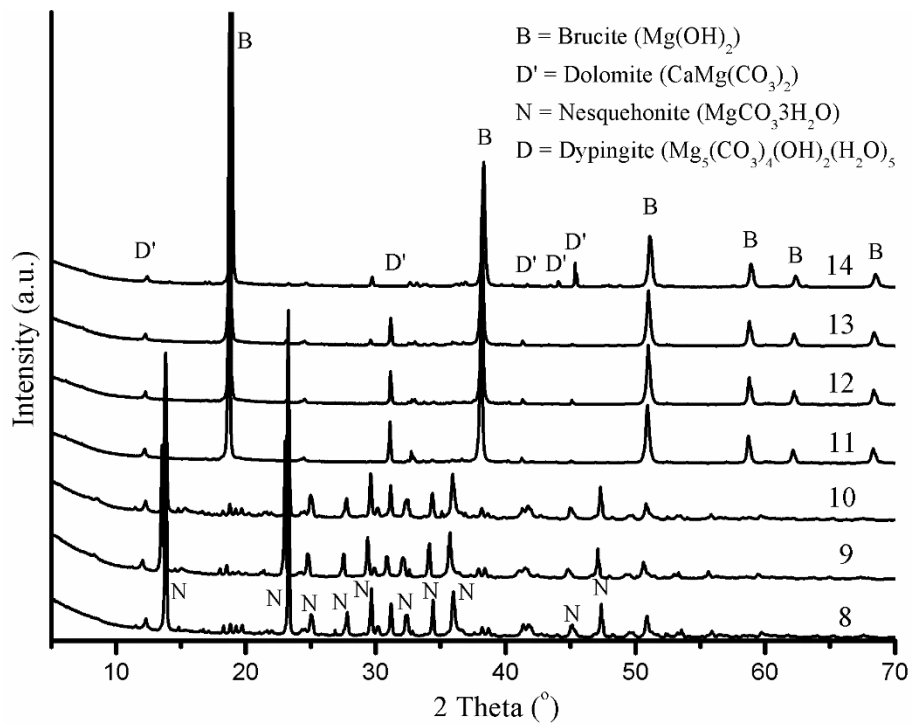
246

247 Figure 6 Typical FESEM images of HMCs obtained at a $\text{Mg}(\text{OH})_2:\text{CO}_2$ molar ratio of 1:2

248

under different pH values of (a) 8, (b) 9, (c) 10 and (d) 11

249



250

251 Figure 7 XRD diffractograms of HMCs obtained at the $\text{Mg}(\text{OH})_2:\text{CO}_2$ molar ratio of 1:2

252

under different pH values

253

254 3.2. Comparison of HMCs synthesized from different source

255 This section aims to provide a comparison of HMCs obtained via reject brine to those of

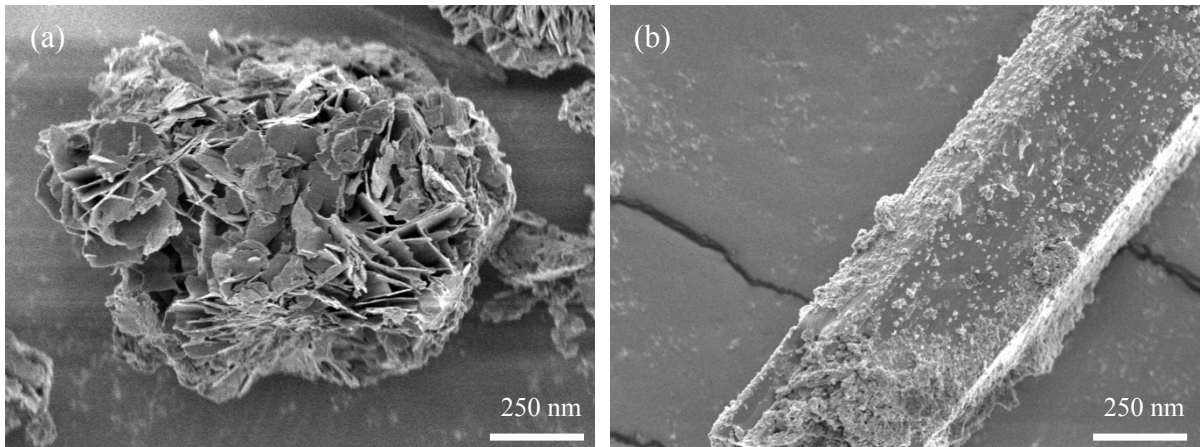
256 chemical Mg(OH)₂ slurry, whose detailed characterization was presented earlier in Section 3.1.
257 The findings presented here aim to use reject brine for the long-term storage of anthropogenic
258 CO₂.

259

260 **3.2.1. Microstructure of HMCs**

261 Figure 8 provides a comparison of the morphologies of HMCs synthesized from Mg(OH)₂
262 slurry and reject brine under a constant pH and Mg(OH)₂:CO₂ molar ratio of 8 and 1:1,
263 respectively. As shown in Figure 8(a), the carbonate crystals obtained via the use of Mg(OH)₂
264 slurry led to a rosette-like morphology. Alternatively, the carbonation of reject brine led to the
265 formation of a needle-like morphology with clear boundaries, as seen in Figure 8(b). The
266 compositions of these rosette- and needle-like particles were confirmed to be nesquehonite and
267 dypingite by XRD patterns revealed in Figure 9, respectively. The formation of different Mg-
268 carbonate phases via the two sources could be associated with the relatively higher reactivity
269 of Mg(OH)₂ prepared from reject brine when compared to that of Mg(OH)₂ slurry (i.e. with a
270 specific surface area of 7.4 vs. 4.8 m²/g as tested by BET analysis). The carbonation of
271 Mg(OH)₂ with a higher reactivity could have capture more CO₂ and enabled the formation of
272 nesquehonite as opposed to dypingite since nesquehonite requires a higher Mg:CO₂ molar ratio
273 as explained in the aforementioned text. This difference in the reactivity of the two samples
274 was also reflected by the absence of the residual brucite peaks in reject brine, as opposed to the
275 clearly defined uncarbonated brucite peaks observed in the Mg(OH)₂ slurry, as seen in Figure
276 9.

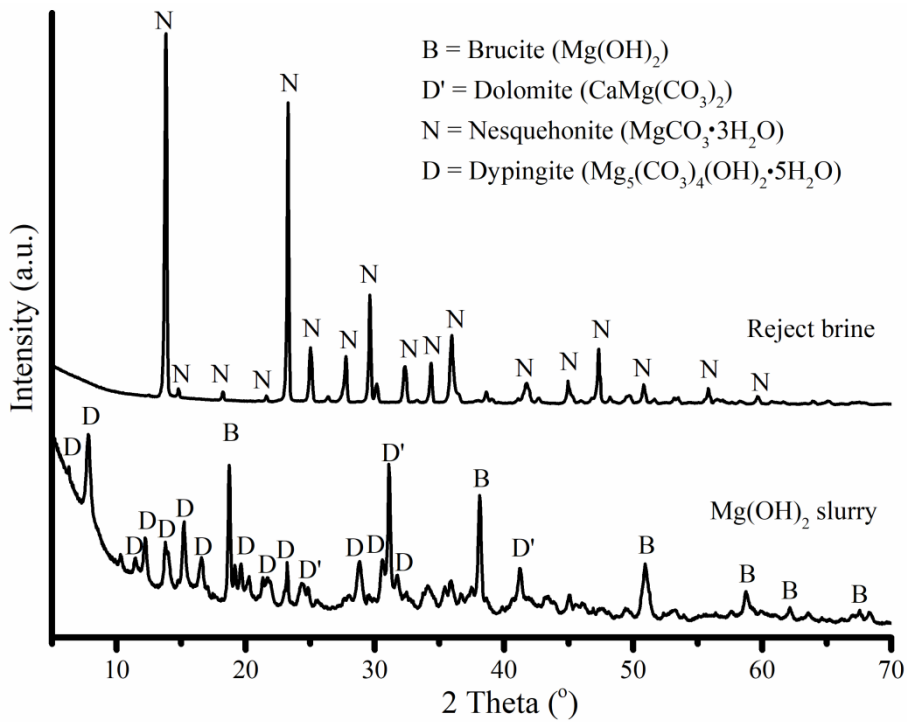
277



278

279 Figure 8 SEM images of HMCs obtained at the $\text{Mg}(\text{OH})_2:\text{CO}_2$ molar ratio of 1:1 under a pH
 280 of 8, showing (a) $\text{Mg}(\text{OH})_2$ slurry and (b) reject brine

281



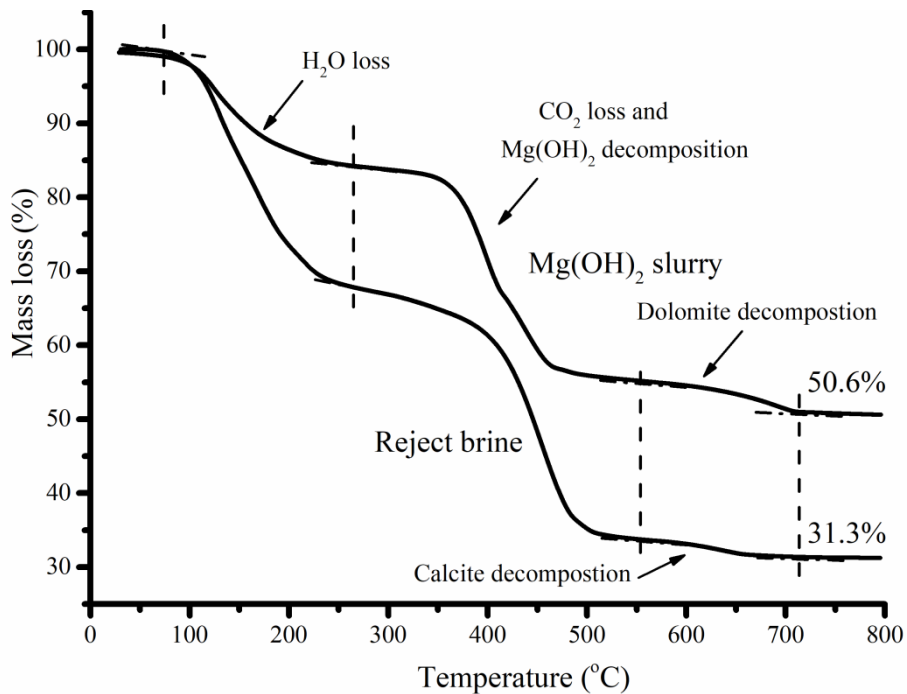
282

283 Figure 9 XRD diffractograms of HMCs obtained from $\text{Mg}(\text{OH})_2$ slurry and reject brine at the
 284 $\text{Mg}(\text{OH})_2:\text{CO}_2$ molar ratio of 1:1 under a pH of 8

285

286 **3.2.2. CO_2 capture and storage**

287 The quantitative analysis of the chemical composition of HMCs and amount of CO₂ used in
 288 their formation was carried out via TG/DTA and ICP-OES analyses. Figure 10 presents the
 289 TG/DTA graphs of HMCs obtained from Mg(OH)₂ slurry and reject brine at the Mg(OH)₂:CO₂
 290 molar ratio of 1:1 and under a pH 8. Both systems demonstrated a similar trend with three
 291 stages of mass loss, which corresponded well with previous studies [36, 54, 55]. Firstly, the
 292 dehydration of HMCs took place at ~100-250 °C, resulting in the loss of H₂O. The second mass
 293 loss occurred between 250 and 550 °C, which was because of the decomposition of
 294 uncarbonated Mg(OH)₂ into MgO as well as the decarbonation of HMCs, resulting in a loss of
 295 H₂O and CO₂. The final mass loss observed between 550 and 700 °C was due to the
 296 decomposition of dolomite and calcite, respectively, which was present as an impurity in the
 297 two systems (i.e. in the form of dolomite in Mg(OH)₂ slurry and calcite in reject brine).
 298



299
 300 Figure 10 Typical TG/DTA curves of HMCs obtained from Mg(OH)₂ slurry and reject brine
 301 at the Mg(OH)₂:CO₂ molar ratio of 1:1 under a pH of 8
 302

303 The chemical composition of the final product was determined via a combination of the results
 304 generated by TG/DTA and ICP-OES, where the recovery rate of Mg^{2+} was measured via ICP-
 305 OES and TG/DTA was used to determine the quantity of each phase derived from XRD results.
 306 Table 2 revealed the composition of the precipitate synthesized via the carbonation of $Mg(OH)_2$
 307 slurry to be composed of 62.1% dypingite and 30.5% uncarbonated brucite. On the other hand,
 308 the carbonation of reject brine led to a precipitate composed of 93.1% nesquehonite and 3.7%
 309 uncarbonated brucite, as detailed in Table 2. These results were used in the calculation of the
 310 percentage of captured CO_2 , which was derived by measuring the mass of CO_2 in the HMCs
 311 (i.e. dypingite/nesquehonite) divided by the initial input of CO_2 degassed to the system at the
 312 $Mg(OH)_2:CO_2$ molar ratio of 1:1. The outcome of these analyses indicated that 43.7% CO_2
 313 could be sequestered in the form of dypingite via the defusing CO_2 into $Mg(OH)_2$ slurry, while
 314 the corresponding ratio of CO_2 sequestered in reject brine was calculated to be 82.6%. The
 315 higher efficiency of CO_2 sequestration achieved via the use of reject brine was associated with
 316 the increased reactivity of $Mg(OH)_2$ synthesized from reject brine. Details of the chemical
 317 composition and the percentage of captured CO_2 were included in the Appendix section.

318

319 Table 2 Chemical composition of HMCs synthesized from $Mg(OH)_2$ slurry and reject brine at
 320 the $Mg(OH)_2:CO_2$ molar ratio of 1:1 under a pH of 8

$Mg(OH)_2$ slurry	Mass (g)	Mass (%)	Reject brine	Mass (g)	Mass (%)
Dypingite	0.6	62.1	Nesquehonite	1.51	93.1
Brucite	0.07	30.5	Brucite	0.06	3.7
Dolomite	0.3	7.4	Calcite	0.05	3.2
CO_2 captured (%)	43.7		CO_2 captured (%)	82.6	

321

322 According to the Paris Agreement, it aims to reduce GHG emissions by 20% (i.e., 7 gigatonnes
 323 CO_2 emission reduction as annual anthropogenic CO_2 emissions is about 35 gigatonnes [56])
 324 in order to hold the increase in the global average temperature to below $2^\circ C$ above pre-

325 industrial levels [56]. According to the International Desalination Association, the global daily
326 production of desalinated water generated by 18,426 desalination plants worldwide exceeds
327 86.8 million m³ [47]. It is estimated that an equivalent amount of reject brine is generated [47].
328 The concentration of Mg²⁺ in reject brine is around 1700 ppm, and thus around 54 million
329 tonnes of Mg could be recovered every year. With a carbon capture and storage rate of 82.6%
330 in the current study, around 45 million tonnes of CO₂ can be sequestered annually. The
331 suggested methodology thus contributes to around 1% of the required CO₂ emission reduction
332 (*i.e.*, 7 gigatonnes) aimed in the Paris Agreement.

333

334 **4. Summary and Conclusions**

335 This study presented the influences of key parameters including the Mg(OH)₂:CO₂ molar ratio,
336 pH, and Mg(OH)₂ source on the synthesis of HMCs through the carbonation of Mg(OH)₂ slurry.
337 The resulting HMCs were characterized via a combination of techniques including XRD,
338 FESEM, and TG/DTA. Main conclusions drawn from this study are summarized below.

- 339 • The carbonation of Mg(OH)₂ slurry under the elevated of Mg(OH)₂:CO₂ molar ratio
340 resulted in the transformation of dypingite to nesquehonite.
- 341 • Increasing the pH from 8 to 10 was found to promote the carbonation process of
342 Mg(OH)₂, resulting in a higher carbonation degree.
- 343 • A specific “house of cards” texture, involving the formation of rosette-like dypingite
344 flakes on the surface of nesquehonite needles, was discovered under elevated pH and
345 Mg(OH)₂:CO₂ ratios conditions. The formation of this structure was associated with to
346 a dissolution-recrystallization-self-assembly growth mechanism as nesquehonite was
347 seen as a precursor for the further nucleation and seeding of hydromagnesite/dypingite
348 on the surface.

- 349 • Carbonation of Mg(OH)₂ slurry synthesized from reject brine led to high yield, high
350 purity, and high carbonation degree (82.6%) HMCs. Reject brine shows high potential
351 to be used for capture and long-term storage of CO₂ in the form of HMCs.

352

353 The use of compressed commercial CO₂ in the research was to provide a pure source to evaluate
354 CO₂ sequestration rate of the synthesized Mg(OH)₂ from desalination reject brine, which
355 served as a model case study. In the ‘real world’ case, different CO₂ sources and collecting
356 methods such as CO₂ generated from factories, coal burning power plants, and municipal solid
357 waste incineration plants, may be used. However, further study is necessary to evaluate CO₂
358 sequestration efficiency of the synthesized Mg(OH)₂ with different CO₂ sources and collecting
359 methods. Furthermore, it is necessary to evaluate the mass, energy, reagents, wastes that
360 come into play in the global process from the life cycle and life cycle cost viewpoint of HMCs
361 synthesized from reject brine.

362

363 **Acknowledgement**

364

365 The authors would like to acknowledge the financial support from the Singapore Ministry of
366 Education Academic Research Fund Tier 2 (MOE2017-T2-1-087 (S)) for the completion of
367 this research project.

368

369 **References**

370 [1] International Energy Agency, Tracking industrial energy efficiency and CO₂ emissions,
371 in, Organisation for Economic Co-operation and Development, 2007.

- 372 [2] V. Mashayekhizadeh, M.H. Ghazanfari, R. Kharrat, M. Dejam, Pore-level observation of
373 free gravity drainage of oil in fractured porous media, *Transport in porous media*, 87
374 (2011) 561-584.
- 375 [3] M. Dejam, M.H. Ghazanfari, V. Mashayekhizadeh, M. Kamyab, Factors affecting the
376 gravity drainage mechanism from a single matrix block in naturally fractured reservoirs,
377 *Special Topics & Reviews in Porous Media: An International Journal*, 2 (2011).
- 378 [4] M. Dejam, M.H. Ghazanfari, M. Kamyab, M. Masihi, The gas-oil gravity drainage model
379 in a single matrix block: a new relationship between relative permeability and capillary
380 pressure functions, *Journal of Porous Media*, 14 (2011).
- 381 [5] V. Mashayekhizadeh, R. Kharrat, M. Ghazanfari, M. Dejam, An experimental
382 investigation of fracture tilt angle effects on frequency and stability of liquid bridges in
383 fractured porous media, *Petroleum Science and Technology*, 30 (2012) 807-816.
- 384 [6] M. Dejam, H. Hassanzadeh, Z. Chen, Semi-analytical solutions for a partially penetrated
385 well with wellbore storage and skin effects in a double-porosity system with a gas cap,
386 *Transport in porous media*, 100 (2013) 159-192.
- 387 [7] J.D. Figueroa, T. Fout, S. Plasynski, H. McIlvried, R.D. Srivastava, Advances in CO₂
388 capture technology - the US department of energy's carbon sequestration program, *Int. J.*
389 *Greenh. Gas Control*, 2 (2008) 9-20.
- 390 [8] T. Morita, J. Robinson, A. Adegbulugbe, J. Alcamo, D. Herbert, E.L. La Rovere, N.
391 Nakicenovic, H. Pitcher, P. Raskin, K. Riahi, Greenhouse gas emission mitigation
392 scenarios and implications, *Climate Change*, (2001) 115-166.
- 393 [9] P. Forster, V. Ramaswamy, P. Artaxo, T. Berntsen, R. Betts, D.W. Fahey, J. Haywood, J.
394 Lean, D.C. Lowe, G. Myhre, Changes in atmospheric constituents and in radiative
395 forcing. Chapter 2, *Climate Change 2007. The Physical Science Basis*, (2007).

- 396 [10] H. Arakawa, M. Aresta, J.N. Armor, M.A. Barteau, E.J. Beckman, A.T. Bell, J.E.
397 Bercaw, C. Creutz, E. Dinjus, D.A. Dixon, K. Domen, D.L. DuBois, J. Eckert, E. Fujita,
398 D.H. Gibson, W.A. Goddard, D.W. Goodman, J. Keller, G.J. Kubas, H.H. Kung, J.E.
399 Lyons, L.E. Manzer, T.J. Marks, K. Morokuma, K.M. Nicholas, R. Periana, L. Que, J.
400 Rostrup-Nielson, W.M.H. Sachtler, L.D. Schmidt, A. Sen, G.A. Somorjai, P.C. Stair,
401 B.R. Stults, W. Tumas, Catalysis research of relevance to carbon management: Progress,
402 challenges, and opportunities, *Chemical Reviews*, 101 (2001) 953-996.
- 403 [11] R. Lal, Soil carbon sequestration impacts on global climate change and food security,
404 *Science*, 304 (2004) 1623-1627.
- 405 [12] R.S. Haszeldine, Carbon capture and storage: How green can black be?, *Science*, 325
406 (2009) 1647-1652.
- 407 [13] A.B. Rao, E.S. Rubin, A technical, economic, and environmental assessment of amine-
408 based CO₂ capture technology for power plant greenhouse gas control, *Environmental*
409 *Science & Technology*, 36 (2002) 4467-4475.
- 410 [14] H.J. Herzog, CO₂ capture, reuse, and sequestration technologies for mitigating global
411 climate change, in, USDOE Federal Energy Technology Center, Morgantown, WV
412 (United States), 1998.
- 413 [15] A. Botha, C.A. Strydom, Preparation of a magnesium hydroxy carbonate from
414 magnesium hydroxide, *Hydrometallurgy*, 62 (2001) 175-183.
- 415 [16] E. Rendek, G. Ducom, P. Germain, Carbon dioxide sequestration in municipal solid
416 waste incinerator (MSWI) bottom ash, *Journal of Hazardous Materials*, 128 (2006) 73-
417 79.
- 418 [17] J.T. Kloprogge, W.N. Martens, L. Nothdurft, L.V. Duong, G.E. Webb, Low temperature
419 synthesis and characterization of nesquehonite, *J. Mater. Sci. Lett.*, 22 (2003) 825-829.

- 420 [18] V. Ferrini, C. De Vito, S. Mignardi, Synthesis of nesquehonite by reaction of gaseous
421 CO₂ with Mg chloride solution: Its potential role in the sequestration of carbon dioxide,
422 Journal of Hazardous Materials, 168 (2009) 832-837.
- 423 [19] E.H. Oelkers, S.R. Gislason, J. Matter, Mineral carbonation of CO₂, Elements, 4 (2008)
424 333-337.
- 425 [20] S.J. Gerdemann, W.K. O'Connor, D.C. Dahlin, L.R. Penner, H. Rush, Ex situ aqueous
426 mineral carbonation, Environmental Science & Technology, 41 (2007) 2587-2593.
- 427 [21] W.J.J. Huijgen, G.J. Witkamp, R.N.J. Comans, Mineral CO₂ sequestration by steel slag
428 carbonation, Environmental Science & Technology, 39 (2005) 9676-9682.
- 429 [22] M. Dejam, H. Hassanzadeh, The role of natural fractures of finite double-porosity
430 aquifers on diffusive leakage of brine during geological storage of CO₂, Int. J. Greenh.
431 Gas Control, 78 (2018) 177-197.
- 432 [23] M. Dejam, H. Hassanzadeh, Diffusive leakage of brine from aquifers during CO₂
433 geological storage, Advances in Water Resources, 111 (2018) 36-57.
- 434 [24] M. Hanchen, V. Prigiobbe, R. Baciocchi, M. Mazzotti, Precipitation in the Mg-carbonate
435 system - effects of temperature and CO₂ pressure, Chemical Engineering Science, 63
436 (2008) 1012-1028.
- 437 [25] W.K. O'Connor, D.C. Dahlin, G.E. Rush, C.L. Dahlin, W.K. Collins, Carbon dioxide
438 sequestration by direct mineral carbonation: process mineralogy of feed and products,
439 Minerals & Metallurgical Processing, 19 (2002) 95-101.
- 440 [26] M.M. Maroto-Valer, D.J. Fauth, M.E. Kuchta, Y. Zhang, J.M. Andrésen, Activation of
441 magnesium rich minerals as carbonation feedstock materials for CO₂ sequestration, Fuel
442 Process. Technol., 86 (2005) 1627-1645.

- 443 [27] A. Sanna, M. Uibu, G. Caramanna, R. Kuusik, M.M. Maroto-Valer, A review of mineral
444 carbonation technologies to sequester CO₂, *Chemical Society Reviews*, 43 (2014) 8049-
445 8080.
- 446 [28] C. Unluer, A. Al-Tabbaa, Enhancing the carbonation of MgO cement porous blocks
447 through improved curing conditions, *Cement and Concrete Research*, 59 (2014) 55-65.
- 448 [29] C. Unluer, A. Al-Tabbaa, Impact of hydrated magnesium carbonate additives on the
449 carbonation of reactive MgO cements, *Cement and Concrete Research*, 54 (2013) 87-97.
- 450 [30] M. Liska, A. Al-Tabbaa, K. Carter, J. Fifield, Scaled-up commercial production of
451 reactive magnesia cement pressed masonry units. Part II: Performance, *Proceedings of
452 the Institution of Civil Engineers-Construction Materials*, 165 (2012b) 225-243.
- 453 [31] M. Liska, A. Al-Tabbaa, K. Carter, J. Fifield, Scaled-up commercial production of
454 reactive magnesium cement pressed masonry units. Part I: Production, *Proceedings of
455 the Institution of Civil Engineers-Construction Materials*, 165 (2012a) 211-223.
- 456 [32] A. Al-Tabbaa, Reactive magnesia cement, *Eco-Efficient Concrete*, (2013) 523-543.
- 457 [33] T.J. Wolery, A software package for geochemical modeling of aqueous systems:
458 package overview and installation guide (version 7.0), Lawrence Livermore National
459 Laboratory Livermore, CA, 1992.
- 460 [34] C. Christ, P. Hostetler, Studies in the system MgO-SiO₂-CO₂-H₂O (II); the activity-
461 product constant of magnesite, *American Journal of Science*, 268 (1970) 439-453.
- 462 [35] J. Kittrick, F. Peryea, Determination of the Gibbs free energy of formation of magnesite
463 by solubility methods, *Soil Science Society of America Journal*, 50 (1986) 243-247.
- 464 [36] P. Ballirano, C. De Vito, S. Mignardi, V. Ferrini, Phase transitions in the Mg-CO₂-H₂O
465 system and the thermal decomposition of dypingite, Mg₅(CO₃)₄(OH)₂·5H₂O:
466 Implications for geosequestration of carbon dioxide, *Chemical Geology*, 340 (2013) 59-
467 67.

- 468 [37] S. Teir, S. Eloneva, C.-J. Fogelholm, R. Zevenhoven, Fixation of carbon dioxide by
469 producing hydromagnesite from serpentinite, *Applied Energy*, 86 (2009) 214-218.
- 470 [38] Y. Wang, Z. Li, G.P. Demopoulos, Controlled precipitation of nesquehonite
471 ($\text{MgCO}_3 \cdot 3\text{H}_2\text{O}$) by the reaction of MgCl_2 with $(\text{NH}_4)_2\text{CO}_3$, *Journal of Crystal Growth*,
472 310 (2008) 1220-1227.
- 473 [39] D.K. Panesar, L. Mo, Properties of binary and ternary reactive MgO mortar blends
474 subjected to CO_2 curing, *Cement and Concrete Composites*, 38 (2013) 40-49.
- 475 [40] Z. Zhang, Y. Zheng, Y. Ni, Z. Liu, J. Chen, X. Liang, Temperature-and pH-dependent
476 morphology and FT-IR analysis of magnesium carbonate hydrates, *The Journal of*
477 *Physical Chemistry B*, 110 (2006) 12969-12973.
- 478 [41] L. Hopkinson, P. Kristova, K. Rutt, G. Cressey, Phase transitions in the system MgO-
479 CO_2 - H_2O during CO_2 degassing of Mg-bearing solutions, *Geochimica Et*
480 *Cosmochimica Acta*, 76 (2012) 1-13.
- 481 [42] P. Ballirano, C. De Vito, V. Ferrini, S. Mignardi, The thermal behaviour and structural
482 stability of nesquehonite, $\text{MgCO}_3 \cdot 3\text{H}_2\text{O}$, evaluated by in situ laboratory parallel-beam
483 X-ray powder diffraction: New constraints on CO_2 sequestration within minerals,
484 *Journal of Hazardous Materials*, 178 (2010) 522-528.
- 485 [43] S. Adham, A. Hussain, J.M. Matar, R. Dores, A. Janson, Application of Membrane
486 Distillation for desalting brines from thermal desalination plants, *Desalination*, 314
487 (2013) 101-108.
- 488 [44] S. Mignardi, C. De Vito, V. Ferrini, R.F. Martin, The efficiency of CO_2 sequestration
489 via carbonate mineralization with simulated wastewaters of high salinity, *Journal of*
490 *Hazardous Materials*, 191 (2011) 49-55.

- 491 [45] Y. Soong, A.L. Goodman, J.R. McCarthy-Jones, J.P. Baltrus, Experimental and
492 simulation studies on mineral trapping of CO₂ with brine, Energy Conversion and
493 Management, 45 (2004) 1845-1859.
- 494 [46] Y. Soong, D.L. Fauth, B.H. Howard, J.R. Jones, D.K. Harrison, A.L. Goodman, M.L.
495 Gray, E.A. Frommell, CO₂ sequestration with brine solution and fly ashes, Energy
496 Conversion and Management, 47 (2006) 1676-1685.
- 497 [47] M.H. El-Naas, Reject brine management, Desalination, Trends and Technologies, (2011)
498 237-252.
- 499 [48] PUB, Desalinated Water, [https:// www.pub.gov.sg /watersupply /fournationaltaps](https://www.pub.gov.sg/watersupply/fournationaltaps)
500 /desalinatedwater.
- 501 [49] H. Dong, E.-H. Yang, C. Unluer, F. Jin, A. Al-Tabbaa, Investigation of the properties of
502 MgO recovered from reject brine obtained from desalination plants, Journal of Cleaner
503 Production, 196 (2018) 100-108.
- 504 [50] H. Dong, C. Unluer, E.-H. Yang, A. Al-Tabbaa, Recovery of reactive MgO from reject
505 brine via the addition of NaOH, Desalination, 429 (2018) 88-95.
- 506 [51] H. Dong, C. Unluer, E.-H. Yang, A. Al-Tabbaa, Synthesis of reactive MgO from reject
507 brine via the addition of NH₄OH, Hydrometallurgy, 169 (2017) 165-172.
- 508 [52] Z.H. Hao, F.L. Du, Synthesis of basic magnesium carbonate microrods with a "house of
509 cards" surface structure using rod-like particle template, Journal of Physics and
510 Chemistry of Solids, 70 (2009) 401-404.
- 511 [53] D. Wu, B.J. Luo, W. Liu, L.C. Wang, Y. Yao, X.P. Huang, Study on the process
512 optimization for intermediate Magnesium Carbonate Tri-hydrate, Advanced Materials
513 Research, 960 (2014) 199-203.

514 [54] R. Dell, S. Weller, The thermal decomposition of nesquehonite $\text{MgCO}_3 \cdot 3\text{H}_2\text{O}$ and
515 magnesium ammonium carbonate $\text{MgCO}_3 \cdot (\text{NH}_4)_2\text{CO}_3 \cdot 4\text{H}_2\text{O}$, Transactions of the
516 Faraday Society, 55 (1959) 2203-2220.

517 [55] J. Lanas, J.I. Alvarez, Dolomitic lime: thermal decomposition of nesquehonite,
518 Thermochimica Acta, 421 (2004) 123-132.

519 [56] UNFCCC, The Paris Agreement Conference of the parties to the UNFCCC, (2015).

520

521

522

523 **Appendix – Chemical composition of HMCs and CO₂ captured percentage**

524

525 HMCs synthesized from Mg(OH)₂ slurry

526 Initially, 0.82 g Mg(OH)₂ is added into 200 ml distil water at a Mg(OH)₂/CO₂ molar ratio of 1.

527 Assuming a purity of 92% for Mg(OH)₂, the remaining 8% impurity is dolomite which does

528 not react or dissolve in the solution. The final precipitates consist of uncarbonated brucite,

529 dypingite and dolomite as supported by XRD results (Figures 5 and 7), which after calcination

530 decompose into MgO, MgO, and CaO·MgO, respectively. Let x and y denote the weights of

531 the uncarbonated brucite and dypingite, respectively. The weight of dolomite is 0.066 g

532 calculated based on 8% of the initial sample weight (i.e., 0.82 g). Residues after the TG/DTA

533 test is 50.6% (Figure 10). Based on the given information, the following equation can be

534 established.

535
$$\frac{\frac{40}{58}x + \frac{40}{96.8}y + 0.82 \times 0.08 \times \frac{96}{184}}{x + y + 0.82 \times 0.08} = 0.506 \quad (A1)$$

536 Furthermore, the concentration of Mg²⁺ in the residue was measured to be 308.4 ppm (0.308

537 g/L) as shown in Table 3. Thus,

538
$$\frac{\frac{24}{58}x + \frac{24}{96.8}y}{0.2} = \frac{\frac{24}{58} \times 0.82 \times 0.92}{0.2} - 0.308$$

539 (A2)

540

541 By solving the two Eqns. (A1) and (A2), the weights of uncarbonated brucite and dypingite are

542 calculated to be 0.27 g and 0.55 g, respectively. The sum of the weights of uncarbonated brucite,

543 dolomite and dypingite was calculated to be 0.89 g, which was higher than 0.46 g of the

544 weighted precipitate as shown in Table 3. This was mainly due to the weight losses during the

545 process of separating the samples from the solution and grinding. The captured CO₂ percentage

546 was calculated by measuring the weight of CO₂ in the HMCs (dypingite) divided by the initial

547 input of CO₂ degassed to the system at the Mg(OH)₂/CO₂ molar ratio of 1, which was calculated
 548 to be 43.7% in consideration of 8% impurity.

549

550 Table A1 Concentration of Mg²⁺ in the residue and final weight of HMCs obtained from
 551 Mg(OH)₂ slurry and reject brine

	Mg ²⁺ in the residue solution (ppm)	Weight of solids (g)
Mg(OH) ₂ slurry	309.9 ± 5.2	0.46 ± 0.20
Reject brine	161.5 ± 9.1	1.24 ± 0.14

552

553 HMCs synthesized from reject brine

554 The same principal applies to HMCs synthesized from the reject brine. The Mg(OH)₂ sample
 555 precipitated from reject brine in the first step contains 6.3% calcite as the impurity which has
 556 been detailed in [50]. The XRD result confirms that HMCs after carbonation of Mg(OH)₂
 557 consisted of nesquehonite, uncarbonated brucite and calcite, which after calcination decompose
 558 into **MgO, MgO and CaO**, respectively. Let x and y denoted the weights of uncarbonated brucite
 559 and nesquehonite, respectively. The weight of calcite is 0.052 g calculated based on 6.3% of
 560 the initial sample weight (i.e., 0.82 g). Residues after the TG/DTA test is 31.3% (Figure 10).
 561 Based on the given information, the following equation can be established.

$$562 \frac{\frac{40}{58}x + \frac{40}{138}y + 0.82 \times 0.063 \times \frac{56}{100}}{x + y + 0.82 \times 0.063} = 0.313 \quad (A3)$$

563 Furthermore, the concentration of Mg²⁺ in the residue brine was measured to be 159.3 ppm
 564 (0.159 g/L) as shown in Table 3. Thus,

$$565 \frac{\frac{24}{58}x + \frac{24}{138}y}{0.2} = \frac{\frac{24}{58} \times 0.82 \times 0.937}{0.2} - 0.159 \quad (A4)$$

566

567 By solving the two Eqns. (A1) and (A2), the weights of uncarbonated brucite and nesquehonite
 568 are calculated to be 0.06 g and 1.51 g, respectively. The captured CO₂ percentage was
 569 calculated by measuring the weight of CO₂ in the HMCs (nesquehonite) divided by the initial

570 input of CO₂ degassed to the system at the Mg(OH)₂/CO₂ molar ratio of 1, which was calculated
571 to be 82.6% in consideration of 6.3% impurity. A successful sequestration of CO₂ into reject
572 brine as HMCs was therefore achieved to obtain an efficiency as high as 82.6%, which was
573 significantly improved compared to the Mg(OH)₂ slurry.

574